Master's Thesis

Variable-density groundwater flow and coupled salt transport models of the Chao Phraya Delta, Thailand

Author: Colin Manz

1st Supervisor: Prof. dr. ir. Harrie-Jan Hendricks-Franssen

2nd Supervisor: dr. ir. Gualbert Oude Essink

November 2018

The following Master of Science Thesis was written in cooperation with Deltares and is in partial fulfilment with the Master of Science program “Applied Geosciences” at RWTH Aachen University.

Title: Variable-density groundwater flow and coupled salt transport models of the Chao Phraya Delta, Thailand

Subtitle: A comparative study on 2D versus 3D variable-density groundwater flow and coupled salt transport models

Student: Colin Manz

Matriculation number: 321706

Specialization: Geophysics - Hydrogeology – Engineering geology

1st Supervisor: Prof. dr. Harrie-Jan Hendricks-Franssen[1,2]

2nd Supervisor: Dr. Gualbert H. P. Oude Essink[3,4]

Additional supervisors: MSc. Joeri van Engelen[3,4] and MSc. Daniel Zamrsky[3,4]

Date: November 2018

1. RWTH Aachen University
2. Forschungszentrum Juelich
3. Utrecht University
4. Deltares

Abstract

In many coastal areas, growing population densities and urbanization have led to extensive groundwater exploitation which has induced irreversible processes such as land subsidence and salt water intrusion. Implementing effective countermeasures requires the identification of at risk areas and a well-developed understanding of relevant processes. For this purpose many studies use numerical variable-density groundwater models to simulate the present situation and future scenarios. Some of these studies have been set up in 2D, due to high complexity and computational restrictions of 3D models. However, it is widely recognized that variable-density flow is a 3D process, as for instance local up-coning following groundwater extractions clearly reveals. This study aims at identifying the magnitude that this simplification in terms of dimensionality has on variable-density groundwater flow for a case study of the Chao Phraya Delta. Therefore, a 3D variable-density groundwater flow coupled with salt transport model was developed using iMOD-SEAWAT for a homogenous and a heterogeneous geological setting. Additionally, thirty-five 2D models were set up using FloPy-SEAWAT with an offset of 5 km along the coastline and spatially inter- and extrapolated to allow for a quantitative comparison. Model conditions as well as input data were kept consistent between 2D and 3D models. As a result, both 3D and 2D variable-density groundwater flow models manage to represent the Chao Phraya Delta to a similar extent. Including influences of groundwater recharge, rivers and drains on the system variations in total fresh groundwater volume are measured at below 0.5 % and 2 % for a homogenous and heterogeneous geological setting respectively. However, salinization patterns reveal profound differences. 2D models show an over-estimation of variable-density groundwater flow due to the neglect of dispersion in the direction not accounted for in a 2D approach, resulting in the fresh-saline interface being pushed up to 2.5 km further inland. The 3D model creates a wider mixing zone than present in the same 2D model which is associated with more space for horizontal salt water intrusions to form and migrate along preferential pathways. Rivers play a vital role in deltaic groundwater systems but are often not included in 2D studies due to the orientation and coverage of rivers. To gain insights to the surface-groundwater interactions for both 2D and 3D models, different river-groundwater interaction scenarios were simulated by changes in riverbed conductance. The 2D models indicate an underestimation of the surface water–groundwater interactions based on the lack of cumulative effects of the river system in 2D. Both 2D and 3D models show fresh groundwater resources to be present in the upper layers of the continental shelf. A long-term paleo simulation indicates that these resources are present in the subsurface and associated with terrestrial groundwater recharge even after a time span of 150 thousand years.

Key words: Variable-density groundwater flow, Chao Phraya Delta, 3D model, 2D model, salt water intrusion, iMOD-SEAWAT, FloPy

Acknowledgements

I'm thankful to my second supervisor Gualbert Oude Essink for giving me the opportunity to conduct my master's thesis at Deltares. When I first sent an email to enquire for this research I was sceptical if it would work out since I had no previous contact to Deltares. But he paved the way with his exceptional enthusiasm and his drive for research. His guidance and continuous efforts lead the way during all parts of this research.

Further I would like to thank my first supervisor Harrie-Jan Hendricks-Franssen for supervising my external master's thesis and even travelling all the way to Utrecht to take part in the introductory meeting of the MSc. Project. This cannot be expected from anyone and therefore I want to express additional appreciation and thankfulness for his efforts. Without him this collaboration could not have been possible.

I'm also highly thankful Joeri van Engelen and Daniel Zamrsky for the continuous guidance and help during every step of the modelling process. Not only were they present at every meeting to add additional ideas and perspectives on the research topic, but also helped me acquire all necessary data and supplied me with important python scripts. Additionally, I want to express my thanks to MSc. Huite Bootsma from Deltares, who was always available for python related questions and many productive discussions. Furthermore, I want to thank my colleagues at Deltares for the pleasant time during my stay in Utrecht.

Table of Contents

List of Abbreviations

AMSL	Above Mean Sea Level
BMSL	Below Mean Sea Level
DEM	Digital elevation model

GEBCO	General Bathymetric Chart of the Oceans
IDW	Inverse Distance Weighting
LB	Lower Bangkok Aquifer
MODFLOW	Modular Three-Dimensional Finite-Difference Ground-Water Flow-Model
MSLR	Mean sea level rise
MT3DMS	Modular Transport Three Dimensional Model Simulator
NB	Nonthaburi Aquifer
NL	Nakorn Luang Aquifer
PD	Phra Padang Aquifer
PN	Pak Nam Aquifer
PT	Phaya Thai Aquifer
SEAWAT	Generic MODFLOW/MT3DMS-based computer program designed to simulate three-dimensional variable-density groundwater flow coupled with multi-species solute and heat transport
SK	Sam Khok Aquifer
SRTM	NASA Shuttle Radar Topographic Mission
SWI	Salt water intrusion
TB	Thon Buri Aquifer
TDS	Total dissolved solids
UB	Upper Bangkok Aquifer
USGS	United States Geological Survey
UTM	Universal Transverse Mercator
WGS	World Geodetic System

List of Figures

1. Introduction

1.1 Introduction

Clean fresh water is essential for consumptive, domestic, industrial and agricultural purposes making it a crucial resource for our everyday lives. Yet, fresh water resources are limited and account to only 2.5 % of the global water resources (Figures 1 and 2). Additionally the majority of global fresh water, approximately 95 % is not easily accessible and stored in the form of deep groundwater, permafrost or bounded in the ice caps (Oki & Kanae, 2006).

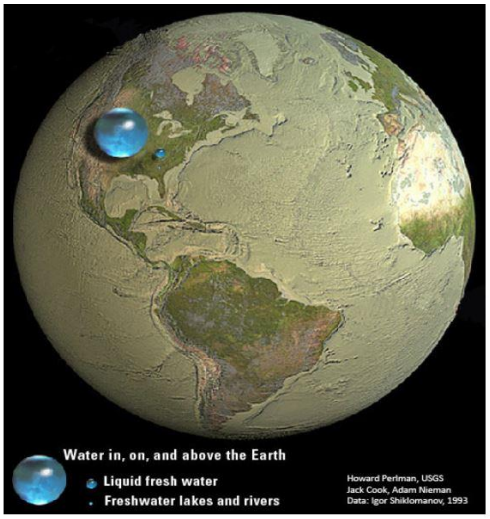

Figure 1: Total water volume vs fresh water volume (source: Perlman, USGS; Shiklomanov, 1993)

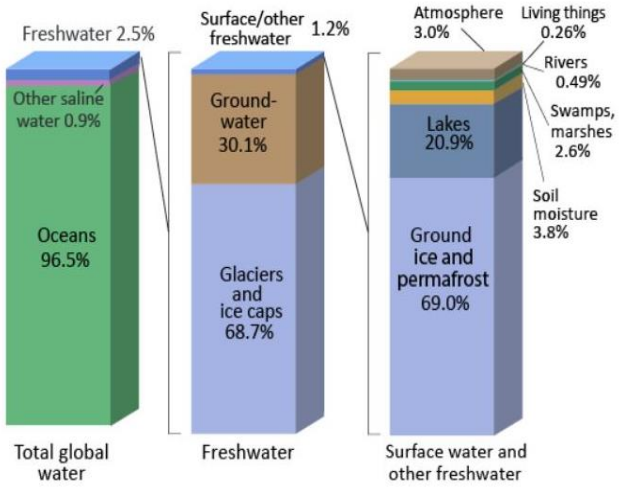

Figure 2: Global water distribution (source: Shiklomanov, 1993)

However, especially in coastal areas worldwide, water demands have been steadily rising during the past decades. This can be attributed to coastal regions exhibiting higher rates of population growth and urbanization than inland counterparts. In particular, low lying deltaic areas have always attracted an abundance of human settlements and activities due to their richness in available resources and favourable logistical settings. Today, approximately 40 % of the world's population lives within 100 km of the coast and 12 out of 16 of the world's biggest cities (with population exceeding 10 million inhabitants) are located in low laying coastal areas (Nicholls, et al., 2007). With current trends in urbanization the demand for fresh water will only become more acute in the coming decades. High water demands and increased pollution of surface water has led to groundwater extractions fuelling the majority of urban water supply systems. In comparison to surface water groundwater has the advantage of high quality and almost no seasonal effects (Oude Essink, 2001). For many coastal aquifers the exploitation of fresh groundwater resources has caused notable declines in water table heights. In the case of Bangkok, excessive over-pumping has led to 65 m piezometric head drawdown (Phien-wej, et al., 2006). Consequently, these areas face immense risks, including overall coastal seawater intrusion, up-coning of deep saline groundwater and irreversible land subsidence. Climate change induced factors such as sea level rise, irregular precipitation patterns, increased occurrences of extreme weather conditions (floods and droughts) are expected to increase the pressure on already vulnerable coastal groundwater resources. Salinization of the groundwater has immense impacts for affected coastal regions leading to loss of water quality, thus making water non-potable and unsuitable for agricultural use (see Table 1).

Table 1: Water salinity classification (based on values obtained from: Oude Essink, Variable-density groundwater flow and coupled salt transport; fresh-saline groundwater in the coastal zone, 2020)

Classification	Salt concentration g/l]	Water type & water usage
Non-saline	<0.6	Drinking and irrigation water
Slightly saline	0.6 - 1.5	Irrigation water
Moderately saline	1.5 - 7	Primary discharge water and groundwater
High saline	7 - 15	Secondary discharge water and groundwater
Very high saline	15 - 35	Very saline groundwater
Brine	>=35	Seawater

To mitigate and ideally avoid the above-mentioned negative effects, countermeasures have to be planned and sustainably implemented. This requires identification of potentially vulnerable areas and a good understanding of the prevailing hydrogeological processes. Numerical groundwater flow models can provide such predictions for different scenarios. In coastal areas groundwater is in direct contact with high saline seawater. The difference in solute concentration results in a contrast in fluid densities which can have a substantial impact on flow behaviour. Therefore, the use of variable-density groundwater flow coupled with salt transport models is required. 3D variable-density groundwater flow models are complex and require intense computational demands. As a result, many studies use 2D models as representatives for the investigated area (Knorr, et al., 2016). However, variable-density groundwater flow is a 3D process. Aquifer geometry (Abarca, et al., 2007), variations in depth of the aquifer boundary, heterogeneity (Hodgkinson, et al., 2007), location of groundwater extractions as well as positioning and orientation of rivers play a major role and attribute to the transport mechanisms with fluid density effects. During the past decade advances in computational capacities and developments of 3D density-dependent flow simulation codes have given the way to a new era of variable-density ground water modelling. Nowadays, many codes are available including SEAWAT (Langevin, et al., 2008) making use of 3D variable-density groundwater flow models practical for a numerous amount of applications.

1.1 Problem definition

The ability to understand, simulate and predict variable-density groundwater flow is a critical challenge for modern hydrogeology (Simmons, 2005). Variable-density groundwater flow in porous media has been investigated by numerous studies, many using numerical models but also through field and laboratory experiments. Some of these studies were set up in 2D as a result of high computational demand of 3D models and limited visualisation possibilities of 3D laboratory experiments (Knorr, et al., 2016). 2D models have the advantage of much lower computational demands and can be used to simulate large timescales in substantially shorter time spans than 3D models. Concurrently, 2D models are built under the assumption that the flow and solute transport mechanisms in the direction orthogonal to the 2D plane are not of major influence and can be neglected. Little attempt has been made to understand the magnitude that this dimensional simplification has on simulated variable-density groundwater flow behaviour. To gain a better understanding, such a simplification could consequently be applied in a real life situation of coastal saltwater intrusion in a deltaic groundwater system under major influences of surface water. To scientifically investigate the deviation between 2D and 3D variable-density groundwater flow models and its impacts on a regional scale groundwater system this research was designed.

1.2 Research objective

This study aims to develop both 2D and 3D variable-density groundwater flow and coupled salt transport models for the Chao Phraya Delta and to compare in what extent 2D and 3D numerical models represent a 3D process such as variable-density groundwater flow. This is done for a real life application on a delta wide scale.

1.2.1 Research questions

Following research questions are addressed:

1. How do 2D and 3D models compare in regard to fresh groundwater quantity and salt distribution pattern?
2. How does the implementation of local geology impact the applicability of 2D and 3D models?
3. How noticeable is the influence of rivers in 2D and 3D models?
4. What density of 2D models is necessary to obtain an accurate and plausible overview of the delta comparable to a 3D model?
5. What interpolation method and procedure is reasonable from a statistical, but also computational perspective?
6. Are 2D models a reasonable approach to access the current situation and capture relevant processes in coastal groundwater systems, more precisely in deltaic areas?

2 Background Information and Literature Review

This chapter provides insights into the basic theories behind groundwater flow and its specifications made for coastal areas, followed by an introduction to the study area.

2.1 Badon Ghijben-Herzberg principle

In coastal areas fresh water aquifers are in direct contact with saline seawater. Typically, buoyancy effects cause freshwater to float over heaver saltwater resulting in a so called fresh/saline wedge of saline seawater penetrating inland below the freshwater (figure 3).

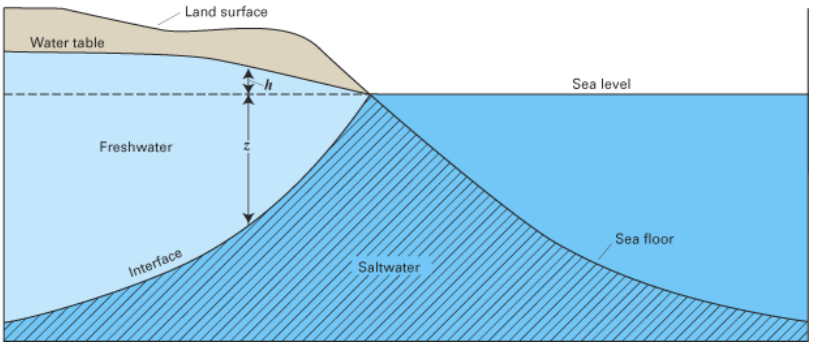

Figure 3: Fresh saline interface in coastal areas (Barlow, 2003)

Badon Ghijben (1889) and Herzberg (1901) were the first to address this phenomenon and found the depth of saltwater to correlate with equivalent fresh water head (Oude Essink, 2001).

$$\rho_s h g = \rho_f (H + h) g \qquad (4)$$

- $\rho_s = denstiy\ saline\ water$
- $\rho_f = \ desnity\ fresh\ water$
- $g = \ gravity$
- $H = depth\ of\ fresh - saline\ interface$
- $h \ = piezometric\ head$

This is referred to as the Badon Ghijben-Herzberg principle. To give an illustration, assuming densities of 1000 g/L for fresh water and 1025 g/L for seawater the density difference is 1/40. Following the approximation the fresh-saline interface can be expected at a depth 40 times the freshwater head above sea level. This approach is limited as it assumes steady-state freshwater flow with a sharp fresh-salt interface and neither considers dispersive nor diffusive mixing effects. The fresh-saline interface usually consists of a gradual transition area.

2.2 Groundwater flow in coastal aquifers

Differences in salinities of ground water and seawater results in density variations which have an effect on groundwater flow behaviour (Oude Essink, 2001). Density-driven free convection can initiate the transport of solutes over large spatial scales in significantly shorter time scales than with diffusion alone (Simmons, et al., 2001). Occurring problems of this phenomenon relevant to coastal aquifers are seen in saltwater up-coning, salt water intrusion, subterranean groundwater discharge, density driven transport in the vadose zone and complex paleo-hydrogeology of sedimentary basins (Simmons, 2005). To emphasise the relevance of variable-density groundwater flow in coastal aquifers a quick illustration: Consider a typical hydraulic gradient for low lying coastal areas of 0.001. That is 1 meter hydraulic head drop over the lateral distance of 1 km. An equal driving force initiated by concentration differences between two fluids would result out of a density difference of only 2 g/L. That is equal to only 5 % of seawater and freshwater concentration difference (Simmons, 2005). The following section gives insights to the theoretical background of variable-density groundwater flow and coupled salt transport.

2.2.1 Groundwater flow equation

Three dimensional groundwater movement of constant density through porous media can be described by an extension of Darcy's Law into three dimensions (McDonald & Harbaugh, 1988), resulting in the following partial- differential equation.

$$\frac{\partial}{\partial x}\left(K_{xx}\frac{\partial h}{\partial x}\right) + \left(\frac{\partial}{\partial y}K_{yy}\frac{\partial h}{\partial y}\right) + \left(\frac{\partial}{\partial z}K_{zz}\frac{\partial h}{\partial z}\right) - W = S_s\frac{\partial h}{\partial t} \qquad (1)$$

- $K_{xx}, K_{yy}, K_{zz} =$ hydraulic conductivities along the x, y and z coordinate $[LT^{-1}]$
- $H =$ piezometric head $[L]$
- $S_s = specific\ storage\ coefficient\ of\ porous\ media\ [L^{-1}]$
- $t = time\ [T]$
- $W = \ volumetric\ flux\ per\ unit\ volume\ representing\ source\frac{and}{or}sinks\ of\ water [T^{-1}]$

2.2.2 Water density

The density of fluids is dependent on pressure, temperature, and solute concentration. In most cases pressure and temperature is relatively constant for groundwater aquifers and the effects on water density can be neglected compared to those induced by changes in solute concentration (Figure 3). Typically the amount of dissolved solids is measured in milligram per litre of total dissolved

solids (TDS). In coastal ground water systems variations in water density are associated primarily with differences in salt concentration as the contact with saline seawater leads to the accumulation of Cl^- ions in the water spectrum.

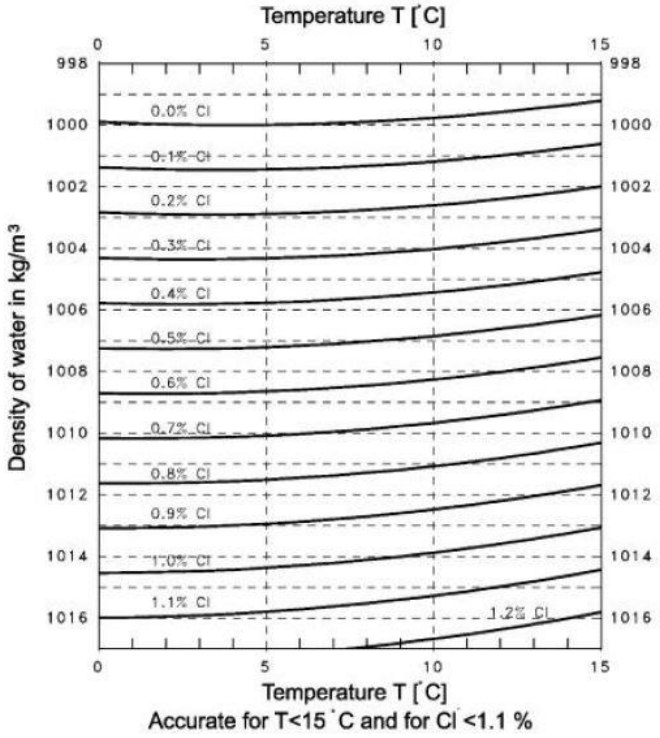

Figure 4: Density of water as a function of chloride content and temperature (Oude Essink, 2001)

2.2.3 Variable-density flow and solute transport

To simulate variable-density groundwater flow, the coupled relationship of solute transport and variable-density flow have to be considered. When solute is transported it initiates a change of the density field itself, which in return affects the ground water flow processes. To account for this, the previously mentioned equation 1 needs to be adjusted (Langevin, et al., 2008):

$$\nabla * \left[\rho K_f \left(\nabla h_f + \frac{\rho - \rho_f}{\rho_f} \nabla z\right)\right] = \rho S_{sf} \frac{\partial_f}{\partial t} + \frac{\partial \rho}{\partial t} \frac{\partial C}{\partial t} - \rho_s q'_s \qquad (2)$$

- $h_f = fresh\ water\ head\ [L]$
- $K_f = fresh\ water\ head\ hydraulic\ conductivity\ tensor$
- $\rho = density\ of\ solute\ [\mathrm{M}L^{-3}]$
- $\rho_f = density\ of\ fluid\ [\mathrm{M}L^{-3}]$
- $q'_s = volumentric\ flow\ rate\ of\ sources\ and\ sinks\ per\ unit\ volume$
- $\nabla = differential\ operator\ (\frac{\partial}{\partial x}, \frac{\partial}{\partial y}, \frac{\partial}{\partial z})$
- $z = elavation\ [L]$
- $S_{sf} = fresh\ water\ specific\ storage\ coifficient\ [L^{-1}]$

Equation 2 has to be solved jointly with the solute transport equation (3) for each transport step (Oude Essink, 2001):

$$\frac{\partial C}{\partial t} = \frac{\partial}{\partial xi}\left(D_{ij}\frac{\partial C}{\partial x_j}\right) - \frac{\partial}{\partial xi}(CV_i) + \frac{(C-C')W}{n_e D}\frac{(C-C')W}{n_e D} \qquad (3)$$

- $D_{ij} = hydrodynamic\ dispersion\ coifficient\ defined\ as\ \mathrm{D} = D^m + D^*\ [\mathrm{M}L^{-3}]$
- $D^m = mechanical\ dispersion\ coefficient$
- $D^* = moecular\ diffusion\ coefficient$
- $V_i = linear\ fluid\ velocity\ in\ direction\ x_i\ [L/T]$
- $C' = solute\ concentration\ of\ water\ entering\ from\ sources\frac{and}{or}sinks$
- $W = sources\ and\ sinks$
- $D = saturated\ thickness\ of\ the\ aquifer$
- $n_e = effective\ porosity$

One of the groundwater simulation codes incorporating variable-density groundwater flow and coupled salt transport is called SEAWAT (Langevin, et al., 2008). It was initially developed by the USGS through the coupling of MODFLOW components to capture groundwater flow and MT3DMS for the solute transport (McDonald, et al., 1988).

Fluid density is calculated by an equation of state using solute transport equation outputs (Langevin & Guo, 2006):

$$\rho_{i,j,k} = +\frac{\partial \rho}{\partial C} * C_{i,j,k}$$

- $\rho_{i,j,k} = fluid\ density\ at\ position\ i,j,k\ [\frac{M}{L^3}]$
- $\rho_f = density\ of\ fresh\ water\ [\frac{M}{L^3}]$
- $C_{i,j,k} = concentration\ of\ the\ fluid\ [\frac{M}{L^3}]$
- $\partial\rho = concentration\ difference\ between\ fluids$

2.3 Variable-density groundwater flow in literature

Variable-density groundwater flow in porous media has been investigated extensively by various studies during the past decades. Field and laboratory experiments were conducted to methodically investigate the general behaviour of variable-density groundwater flow (e.g. Xie et al., 2010; Johannsen et al., 2006). Van Dam et al. 2009 conducted the first field documentation of natural free convection induced by density contrasts. Variable-density groundwater modelling has been applied for 3D cases, modelling regional scale groundwater systems (Oude Essink, 2001), and has proven to be practical for paleo reconstruction modelling of coastal areas (Delsman, et al., 2014). Numerous studies have documented the notably semi chaotic and transient character of density driven flow (Flowers & Hunt, 2007; Beinhorn, et al., 2005). Density driven convection can become unstable under certain settings depending on permeability, porosity and ratio of flow velocities or densities of intruding water to resident water. Unstable variable-density groundwater flow is characterized by the formation of instabilities with constantly varying densities in space time. This phenomenon results in horizontal and vertical distribution of solutes (Flowers & Hunt, 2007). The documented unstable behaviour may result in an increased rate of saltwater intrusion on the regional scale. The role of heterogeneity on variable-density groundwater flow has been noted by Simmons et al. (2001) who demonstrated that the onset and subsequent growth or decay of convective instabilities is intimately related to the structure of heterogeneous porous media. Heterogeneity is stated to serve

as the triggering mechanism for the onset of instabilities and also decides whether instabilities will grow or decay after they have been generated (Simmons, et al., 2001). Various studies have linked heterogeneity to variable-density groundwater flow behaviour. Ghassemi et al. (2000) found aquifer heterogeneities to be essential for a successful reconstruction of field observations through numerical models. Oki et al. (1998) indicated that aquifer heterogeneity controlled mixing zone shape and width.

Further Hodgkinson et al. (2007) concluded that the distribution and thickness of low permeable sediments directly controlled freshwater lens volume. It has also been noticed that the scale of heterogeneity plays an important role (Werner, et al., 2013). Randomly distributed small-scale heterogeneities only have minor impact on the lateral extent of the mixing zone. Macroscopic variations however have a much greater influence and can lead to major changes in the extent and shape of the mixing zone (Werner, et al., 2013). Abarca et al. (2007) pointed out the influence of aquifer geometries on variable-density groundwater flow. The study revealed changes in slope and elevation of water bearing layers to have immense impacts on the distribution of salt and freshwater, even creating quasi horizontal circulation cells for intruding saltwater. They concluded for aquifers with varying aquifer geomorphology a 3D approach is essential to capture variable-density groundwater flow correctly. Although on small scales in homogenous media 2D models have proven to reproduce 3D results to an acceptable degree. Knorr et al. (2018) has demonstrated the reproduction of multiple 3D homogenous sand column experiments through 2D asymmetric and 3D numerical models. Mass recovery rates of 2D and 3D numerical models were between 77 % and 99 % depending on variations in flow velocities and density contrasts.

2.4 Study area

The main area of interest in this study is located in Southeast Asia covering the central part of Thailand including the Bay of Bangkok, a small inlet of the Gulf of Thailand (see Figure 5). The present landform can be characterized by its relatively even morphology and low elevation height(Gupta, et al., 1985). It is known as the Lower Central Plain. It spans 175 km in width and is bordered by steep sloping carbonate mountain ranges to the West and the Khorat Plateau on the East (Phien-wej, et al., 2006). To the south it is bounded by the Gulf of Thailand, expands 200 km to the north where it is bordered by a series of hills separating it from the Upper Central Plain.

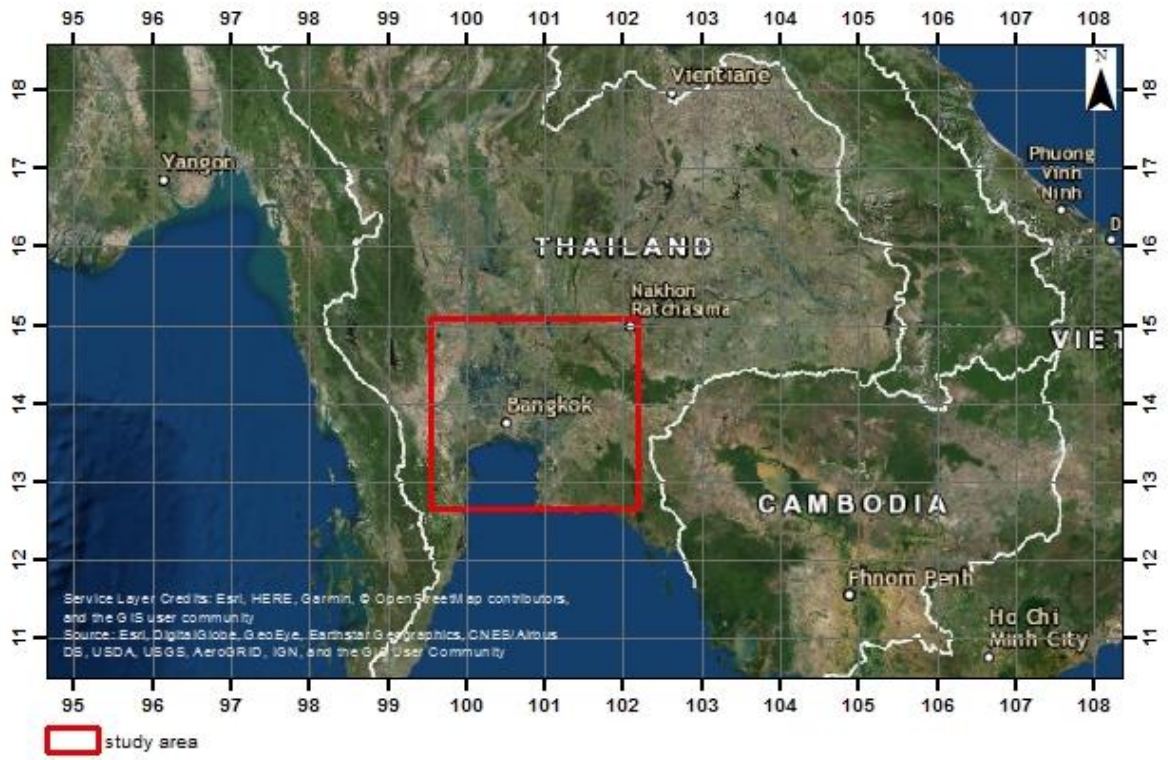

Figure 5: Location of study area (geographic coordinate system: WGS 1984)

The Chao Phraya is the biggest river in the Lower Central Plain. It is supplied by 5 major tributaries including the Pak Sak, Nam, Yom, Wang Ping, Sakae Krang and drains into the Gulf of Thailand forming the Chao Phraya delta (Figure 6). The Chao Phraya river basin has a drainage area of 21,725 km^2 generating an average runoff of 117.0 m3/s for the Chao Phraya River (measured at Sang Khla Buri District, Chainat Province) (Molle & François, 2005).

Figure 6: Chao Phraya River and its tributaries (source: Wikimedia Commons, 2008)

2.4.1 Climate

The climate can be described as humid and tropical with 3 main seasons. The Southwest Monsoon Season ranging from mid-May to mid-October followed by the Northeast Monsoon Season from mid-October to mid-February and the pre-Monsoon from mid-February to mid-May (Stoecker, et al., 2013). Precipitation cycles are greatly dominated by the presence of wet and dry season. According to hydrological data average annual precipitation ranges between 1100 mm and 1600 mm. Average monthly temperature is measured to be between 23˚C and 33 ˚C (Stoecker, et al., 2013).

2.4.2 Urbanization

Thailand's capital city Bangkok is located at the heart of the Chao Phraya delta 25km north of the coastline. Population and urbanized area have expanded rapidly over the past decade along with groundwater extractions. Since 2000, population growth rates have continued to increase by 2.5 times the rates from 1980 to 2000 (Figure 7). As a result by year 2016 Bangkok boasted a population of 8 million, the metropolitan area 15 million. Population densities account to 5300 and 5900 inhabitants per km^2, respectively. The fast development has created immense pressure on local water resources. Groundwater extractions have led to up to 65 m of hydraulic head drawdown creating high subsidence rates as high as 120 mm/year (Phien-wej, et al., 2006) and a wide spread salinization of the productive aquifers (Stoecker, et al., 2013).

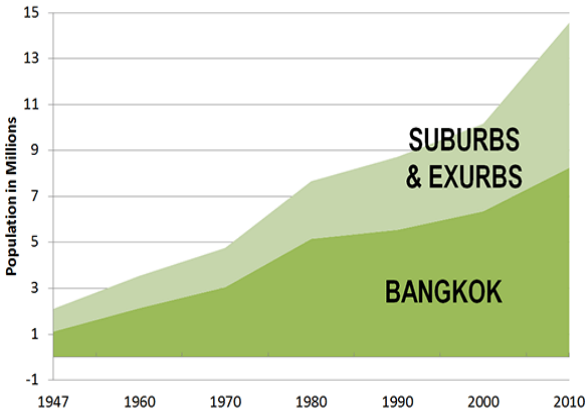

Figure 7: Population development of the Bangkok region between 1947 and 2010 (source: New Geography, 2012)

2.4.3 Geology/Hydrogeology

The geological structure of the study area is mainly characterized by a sedimentary basin known as the Chao Phraya Basin, which forms the subsurface of the Lower Central Plain and Gulf of Thailand. According to Nutalaya and Rau (1987) fault block tectonics during the late Pilocene-Pleistocene resulted in a north south trending depression lowering the basement rock into a graben. The basin generally slopes towards the basin central axis which is located above the Chao Phraya River and inclines towards the Gulf of Thailand (Gupta, 1985). The depth and lithology of the bedrock formation are not well documented due to the thick coverage with unconsolidated sediments. The depositional environment has been determined by a series of transgression and regression events (Figure 8). Accumulated sediments mainly consist of fluviatile and marine deposits of the Chao Phraya River delta.

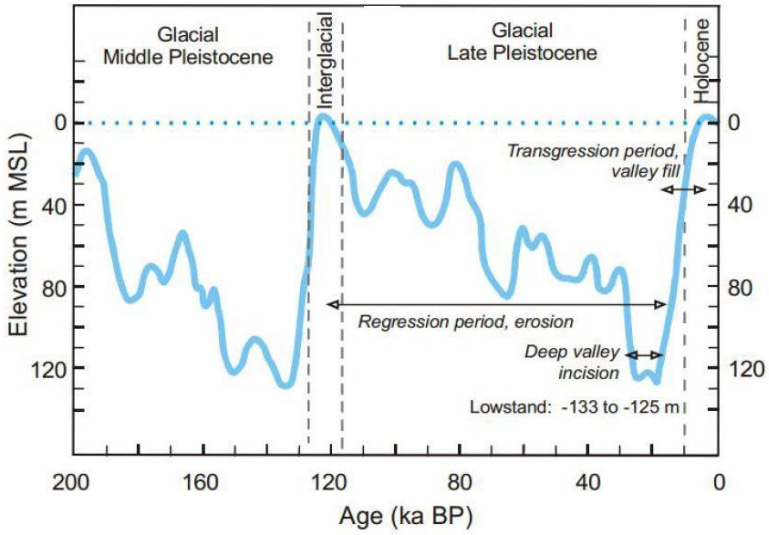

Figure 8: Sea-level curve during the past 200 kyrs (Waelbroeck, et al., 2002)

In the late Pleistocene, the sea level was approximately 100 m below its current state (Sinsakul, 2000). As a result the Gulf of Thailand was completely dry and the shoreline was far from its present location. According to Sinsakul (2000) it was a period of erosion and weathering. Eroded sediments were transported by fluviatile systems and merged with complex alluvial fans. In this time Pleistocene sands which make up the major productive aquifers were deposited. During the Holocene epoch the sea invaded the Gulf of Thailand. Records of transgression start at about 8000 y. B.P. and reach its maximum of about 4 m A.S.L. at approximately 6000 y. B.P.. The arisen Holocene sea covered big parts of the present Lower Central Plain and is reported to have reached as far as the Chainat area (Sinsakul, 2000). The depositional environment was characterized by tidal flats with mangrove forest, creeks and estuaries with daily tides producing marine clays and intertidal flat deposits. The extent of the tidal flats can be observed in Figure 9.

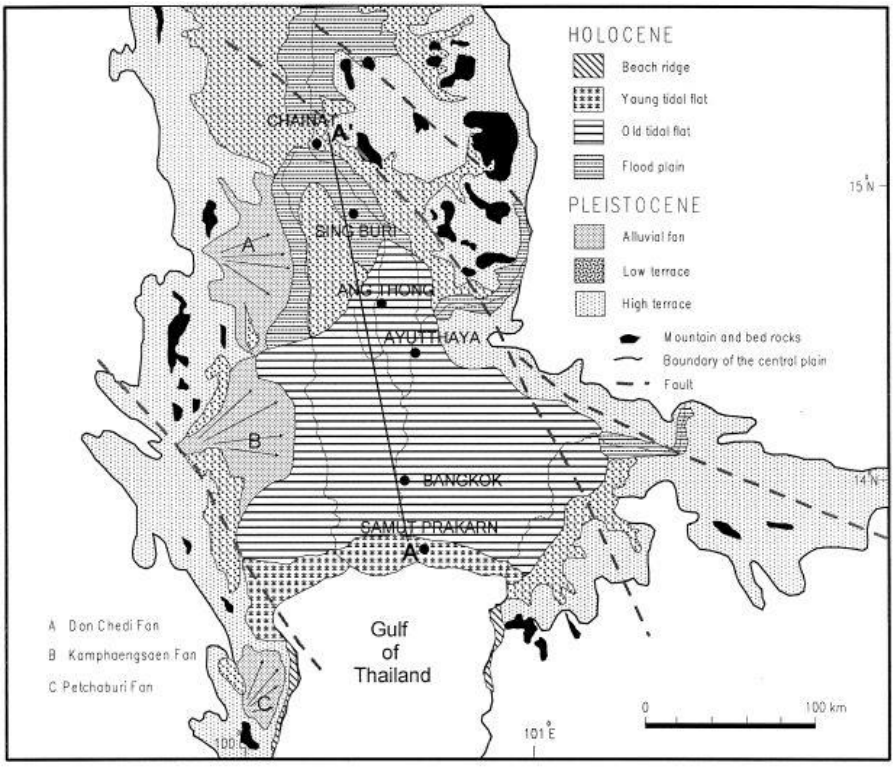

Figure 9: Chao Phraya Delta system with Holocene and Pleistocene depositional environments (Sinsakul, 2000)

The sea has retreated from the Lower Central Plain during the last 3000 years reaching its current level about 1500 years ago and leaving behind a soft clay layer known as Bangkok Clay. Thicknesses of the deposited marine clays vary spatially, but range up to 25 m for the Bangkok metropolitan area. The upper 600 m of Pleistocene and Holocene deposits are subdivided into eight complex water bearing unconsolidated sand and gravel aquifers (Figure 10) separated by thick clay layers.

The confined aquifers can be listed from top to bottom as following:

1. **Bangkok aquifer**
2. **Phra Pradang aquifer**
3. **Nakorn Luang aquifer**
4. **Nonthaburi aquifer**
5. **Sam Khok aquifer**
6. **Phaya Thai aquifer**
7. **Thon Buri aquifer**
8. **Pak Nam aquifer**

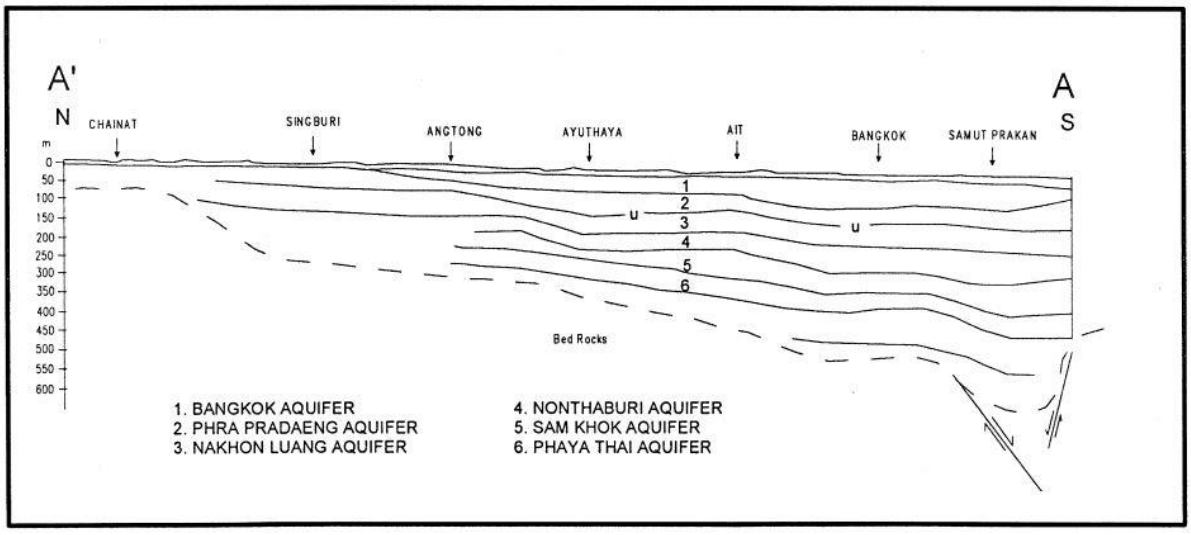

Figure 10: North-South profile of the Chao Phraya Delta hydrogeological system (Sinsakul, 2000)

3 Research Methodology

This chapter provides insights to the data collection and processing as well as an illustration of the initial model set up for 2D and 3D models.

3.1 General Methodology

The general steps can be split up into the following categories:

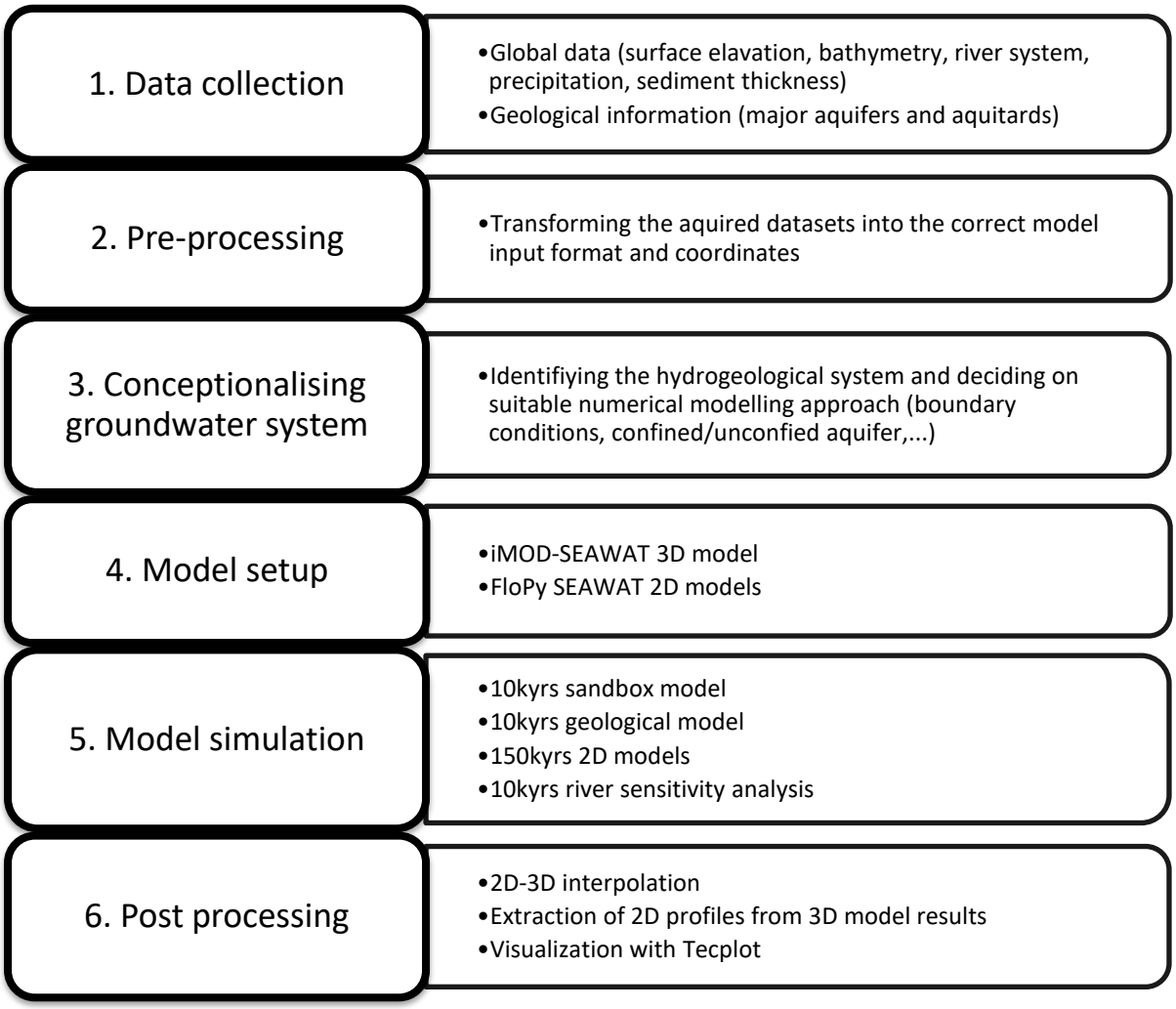

Figure 11: Methodological research steps

Table 2: Datasets

Input	Database
Bathymetry & elevation	*GEBCO 2014* (Weatherall, et al., 2015)
River network	*GAIA 2013* (Andreadis, et al., 2013)
Surface lithology	*Global surface lithology* (Hartmann & Moosdorf, 2012)
Bedrock depth	*Regolith thickness* (Zamrsky, et al., 2018)
Precipitation	*WorldClim 2* (Fick & Hijmans, 2017)
Hydrogeological properties	*Giao et al. 1998*
Holocene sediment distribution & thickness	*Online GIS database (CCOP Geoinformation Sharing Infrastructure)*

3.2 Data collection and pre-processing

An extensive amount of input data was used for construction of the numerical groundwater models. Table 2 provides an overview of all the collected datasets. A detailed description of each individual dataset is provided in the following section. All listed datasets were used for the setup of both 2D and 3D models.

3.2.1 Bathymetry and digital elevation model

Bathymetry describes the underwater surface of large water bodies such as lakes, seas and oceans. Information on bathymetry has been combined with a digital elevation model (DEM) representing the land topography by Weatherall et al. (2015) to achieve global coverage of surface elevation and depth relative to current sea level. The resulting GEBCO (General Bathymetric Chart of the Oceans) dataset consists of a global relief model with a resolution of 30 arcsecs (approximately 1x1km). In this study the GEBCO 2014 dataset was used as the top elevation of the system (Weatherall, et al., 2015).

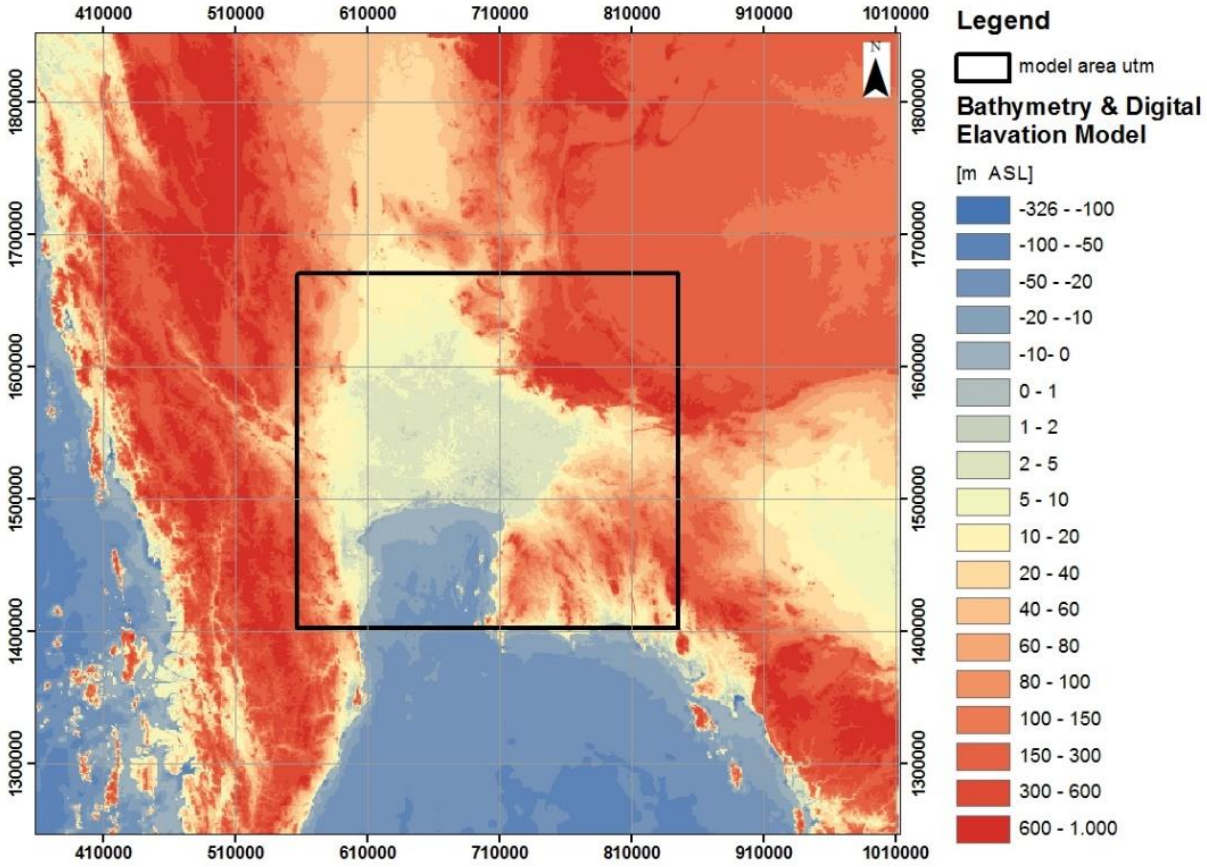

Figure 12: Relief of the study area (WGS 1984 UTM Zone 47N)

3.2.2 Rivers

In this study the GAIA river network (Andreadis, et al., 2013) was used to incorporate rivers into the model. It contains global coverage of river location, river width and river depth (Figure 13). An important factor in estimating the flow relationship between river and aquifer is the river streambed conductance. It is assumed that all measurable river-aquifer losses are due to the streambed itself.

River streambed conductance can be derived from the Darcy's law and is simplified by the equation (McDonald & Harbaugh, 1988):

$$C = K * l * w/b$$

With river conductance C (m^2/d) depending on the hydraulic conductivity of the river bed K (m/s) and its thickness b (m), as well as the area covered by the river expressed through river length l (m) and river width w (m). Since the hydraulic properties of the riverbed are unknown a simplification has to be made. For the model cell size of $1km^2$ the factor 10 multiplied with the river width has proven to produce a rough estimation (Mulder, 2018). For the 2D models the river conductance was reduced according to the difference in cell size.

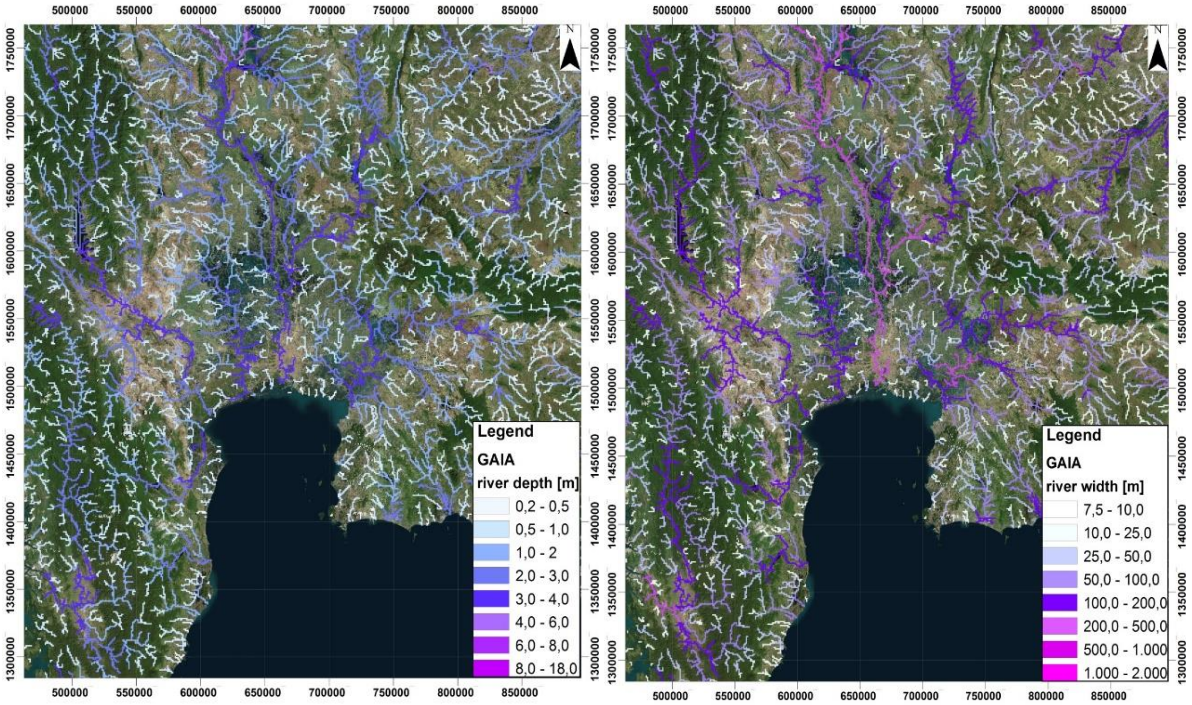

Figure 13: GAIA river network. Left side: river depth; right side: river width (WGS 1984 UTM Zone 47N)

3.2.3 Precipitation and groundwater recharge

Precipitation was estimated based off the WorldClim version 2 dataset (Fick & Hijmans, 2017). It utilizes observed climate data from over 9000 and up to 60 000 weather stations over a time span of 30 years (1970 to 2000) and provides monthly data for minimum, mean, and maximum precipitation with a resolution of ~1 km². Monthly average precipitation was converted from millimetres per months to meters per day and exported in IDF raster format. Estimating groundwater recharge is a complex process as it depends on wide range of factors. Climate factors such as precipitation and evapotranspiration and their spatial and temporal distribution play a role, but also land use and soil characterises such as infiltration capacity play have an impact and can affect groundwater recharge substantially. In this case we assumed the delta area is a surface water-driven system which is also supported by the presence of a sealing clay layer. According to Gupta (1985) a hydrologic balance study carried out by the Asian Institute of Technology determined the groundwater recharge of the basin to be only 3 % of the annual precipitation. This confirms our previous assumption. Consequently, precipitation was multiplied by the factor 0.03 and assigned to the land area of the model.

3.2.4 Geology

3.2.4.1 Bedrock

The most productive aquifers used for groundwater abstraction are usually formed by unconsolidated sediments. These formations overlay a low permeable (low porosity and low hydraulic conductivity) bedrock formations. Therefore, these underlying rocks are considered to be the lower no-flow boundary in groundwater flow models. Further important input information for implementing a groundwater flow model is the thickness of the unconsolidated sediments. For this study a dataset published by Daniel Zamrsky a PhD researcher at Deltares and Utrecht University was used (Zamrsky, et al., 2018). It estimates the thickness of unconsolidated sediments for coastal areas based on combined utilization of land surface topography and ocean bathymetry (GEBCO_2015), aquifer thickness estimations from a global hydrological model (De Graaf, et al., 2015) and surface lithology (Hartmann & Moosdorf, 2012).

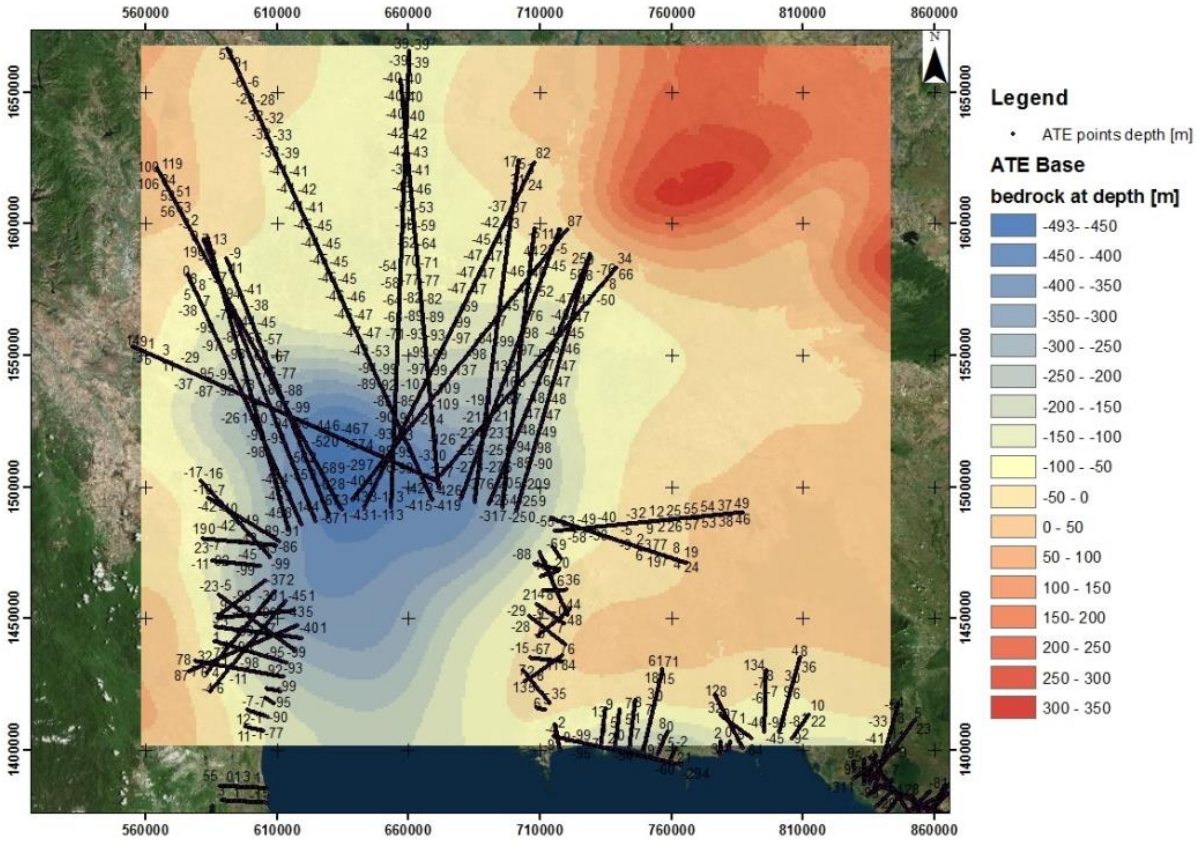

Figure 14: Bedrock depth and ATE points in the model area (WGS 1984 UTM Zone 47N)

The bedrock depths are calculated along the coastline for various grids formed between coastal points (every 5 km) and inland as well as offshore anchor points. Maximum depths of unconsolidated sediments are estimated at 450 m to 600 m according to Phien-wej et al. (2006) and Giao et al. (1998). After visual inspection and consideration of literature values one point with a depth of -1283 m was excluded from the data set due to overestimation. All the other points were combined and spatially interpolated to form a surface covering the model area using ArcGIS implemented simple kriging algorithm. Additionally, the smoothing mechanism Focal Statistics was

applied with a rectangular 10x10 neighbourhood for a more uniform and realistic delta geometry. Comparison of the output plain with DEM revealed some areas of the interpolated bedrock depth to surpass the surface elevation height. To avoid numerical issues a minimum cumulative sediment thickness of 15 m was assigned to all cells possessing < 15 m between surface elevation and bedrock depth. The interpolated sediment basin has a maximum depth of 493 m and its major volume is located in the central parts of the delta, with the sediment thickness thinning out drastically towards the northern and southern boundary (Figure 14). The estimation corresponds well to available literature data for the central parts of the delta (Phien-wej, et al., 2006).

3.2.4.2 Geological *model*

Despite many publications providing a good general overview of the hydrogeological situation (see chapter 2.4.3), usable open source data on the Bangkok aquifer system is very limited. Only five bore logs indicating aquifer and aquitard horizons could be found in available literature, making the construction of geological features using bore logs impossible for such a large area. Due to this reason a different approach utilizing the available information had to be considered. General orientation and sequence of geological layers is well documented through various schematizations and sketches, as shown in Figure 15.

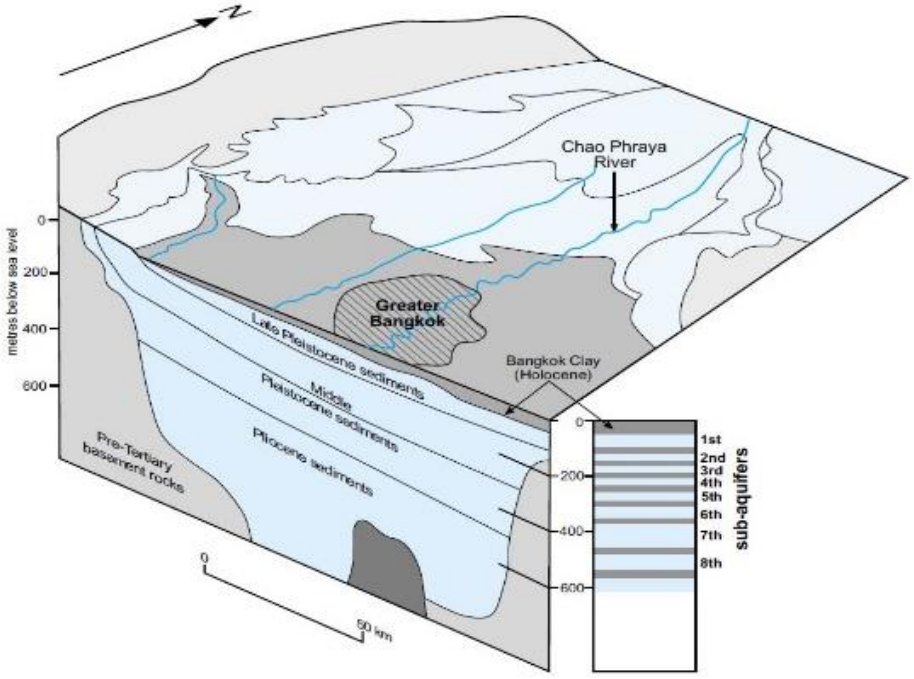

Figure 15: Structure of the Chao Phraya Basin (Phien-wej, et al., 2006)

The observed basin structure can be characterized by east-west semi horizontal layers, slightly dipping towards the basin axis, and cropping out at the eastern and western flanks. According to Gupta, et al. (1985) only the 2nd to 5th layer crop out at the basin flanks. This is of importance as the areas with outcropping sand and gravel aquifers are those generating the bulk groundwater recharge into to the system. All other surface areas are covered by clay layers that are sealing the top of the system. In north-southern direction cross sections indicate a slight dip towards the Gulf of Thailand. For simplification purposes all continuous layers were assumed to be horizontal in N-S direction for the model. The CCOP Geoinformation Sharing Infrastructure for East and Southeast

Asia (GSi) Project offers a publicly available online database with maps containing the distribution and thickness of quaternary sediment facies for the Chao Phraya River Basin. A raster file containing coverage and thickness of Holocene and Pleistocene sediments was generated from the CCOP database. Detailed information on the thickness was only available for the Bangkok Clay. The outer area representing outcropping Pleistocene sediments was calculated for the 2nd to 5th layer based on the estimated thickness and dipping angle.

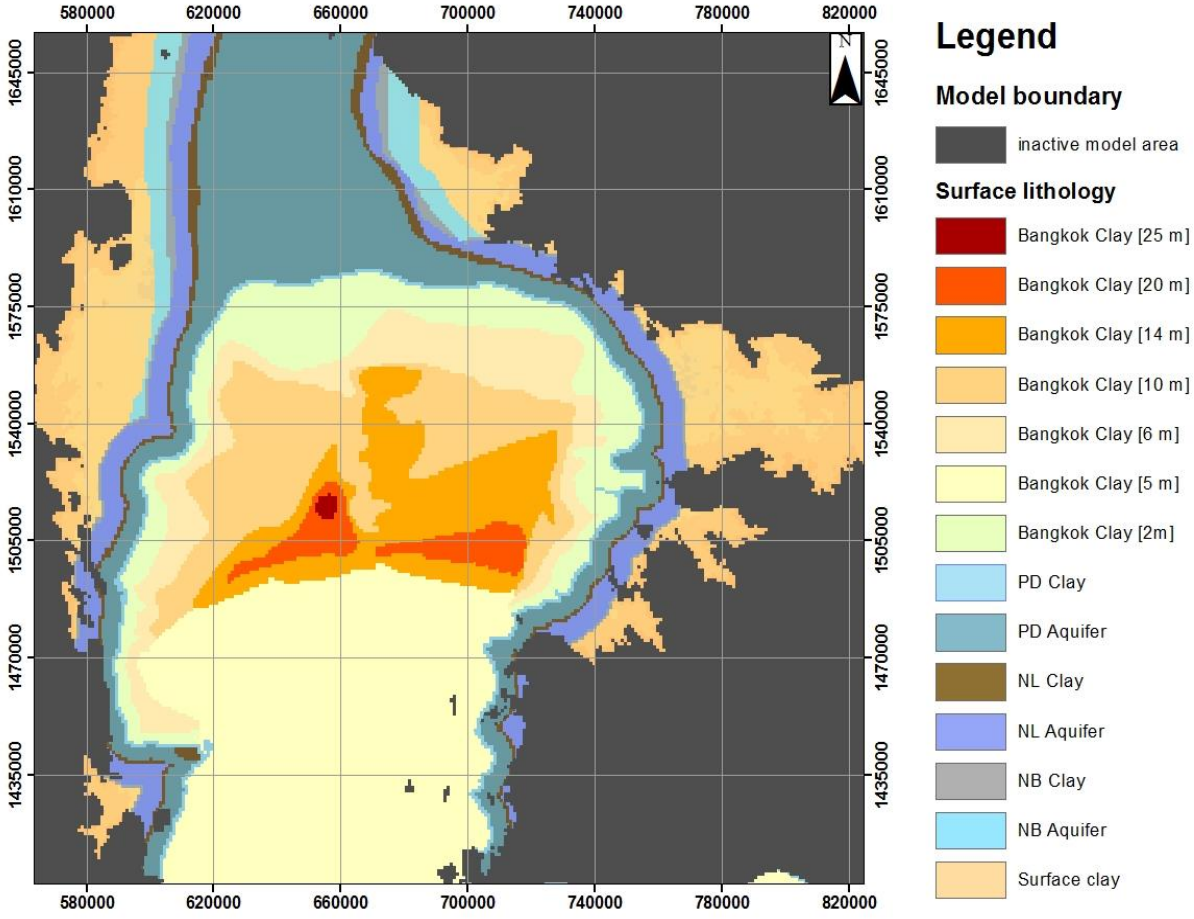

Figure 16: Distribution of Pleistocene and Holocene sediments and their facies (coordinate system: WGS 1984 UTM Zone 47N)

An important aspect to consider for the construction of the geological model is a possible presence of an open or closed system offshore. In other words, if the hydrogeological system is sealed from the top by a clay layer the interactions between groundwater and seawater are limited. On the other hand, if the system is open a free interaction between saline and fresh groundwater bodies can take place. The geophysical service company Fugro conducted seismic measurements in the Gulf of Thailand approximately 70 km south of the coastline. Processed seismic images for depths between -55 and -82 m MSL shows fine grained material underlain by sand (Figure 15). Puchala et al. (2001) interpreted the observations as terrestrial and fluviatile sediments deposited during the Pleistocene which are overlain by marine clay very similar to Bangkok Clay (Figure 16). A similar depositional environment can be assumed as the submerged seabed has a relatable geological layer sequence compared those typically found in the Bangkok area (Puchała, et al., 2011). According to this a closed system was assumed for the geological model.

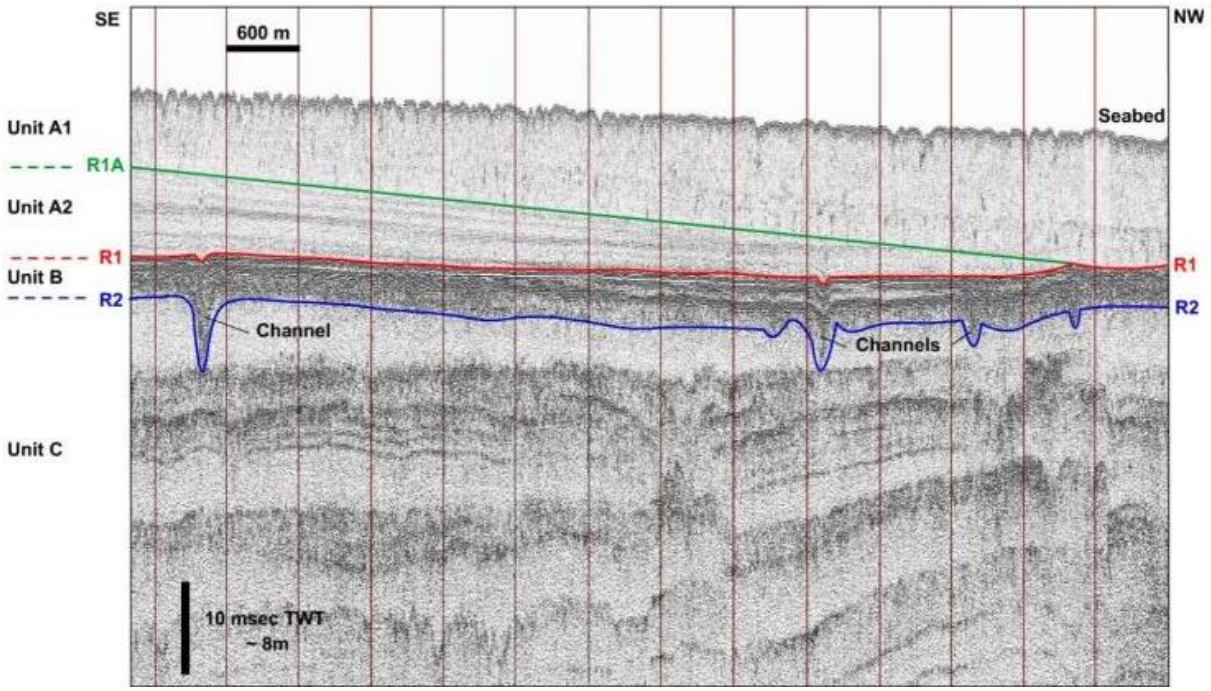

Figure 17: Seismic images showing major units and reflectors of the central part of the Gulf of Thailand. (Puchała, et al., 2011)

			Lower Central Plain, Thailand		Gulf of Thailand (west basin)	Gulf of Thailand (central south basin)	Central Sunda Shelf / South China Sea
	Formations		(Dheeradilok 1995)	(Sinsakul 2000, Wongsomsak & Theyapunte 1987, Biswas 1973)	(this paper)	(Puchala et al 2011, this paper)	(Hanebuth et al 2002)
HOLOCENE	Bangkok Clay Formation		Top soil alluvial	Weathered clay and recent flood sediments	**Unit A1**	**Unit A1**	**Unit 1**
		Soft Clay Mem	Subtidal shells & peat (4-5 kyr)	Intertidal sediments including lenses of basal peat	Condensed modern marine mud	Condensed modern marine mud	Marine mud, partially transgressive (tidal to shelf)
			Intertidal sediments	Marine clay including lenses of basal peat	(0-6.4 kyr)	(0-8.3 kyr)	(0-11 kyr)
						Unit A2 Muddy prodelta	
					R1 ravinement surface	**R1** ravinement surface (10.3-10.6 kyr)	Coastal plain, tidal env. (~12 kyr) Mangrove swamp (~12.5 kyr)
			Unconformity		/ Inferred fluvial deposits / Subaerial hiatus / Soil development within Unit B	/ Inferred fluvial deposits / Subaerial hiatus / Soil development within Unit B	**Unit 2 - Unit 3** Transgressive, terrestial to estuarine sediments (14-19 kyr)
							Unconformity β
							Soil development (21-23 kyr)
UPPER PLEISTOCENE	Chao Phaya Formation				**Unit B** Stiff sandy silt with carbonate-ferruginous concretions mottles of lateritic soil	**Unit B** Stiff sandy silt with goethite/lepidocrocite concretions mottles of lateritic soil	**Unit 4** Nearshore, marine, partially terrestrial sediments (30-45 kyr)
		Stiff Clay Mem	Estuarine	Stiff clay with iron and manganese pisolitic concretions and red and orange mottles of lateritic soil			
			Deltaic sand/silt		**Unit C** Alluvial, fluvial and marine sediments (common channels)	**Unit C** Alluvial, fluvial and marine sediments (common channels)	
			Lacustrine marl formation	Alluvial and fluvial complex			**Unit 5 - Unit 9** (Older than 50 kyr)

Figure 18: Interpretation of the seismic surveys for the shallow parts of the central area in the Gulf of Thailand and their correlation with adjacent areas in the Lower Central Plain (Puchala, et al., 2011).

Consequently, the layers were horizontally extended into the Gulf of Thailand and a clay layer of 5 m thickness was assigned to the top of the system for the sea area following the measurements of Puchala, et al. 2011 and Puchala and Porebski, 2014. Giao, et al. (1998) characterized the Bangkok groundwater system using values obtained through groundwater well productivity data. Estimated average hydraulic conductivity, specific storage coefficient and average layer thickness are shown in Table 3.

Table 3: Hydrogeological properties for Bangkok aquifer system based on values by Giao, et al. (1998)

Layer	Geological Layer	Bottom Depth [m]	Average Thickness [%]	Hydraulic Conductivity Values [m/d]	Specific Storage Coefficient
1	Upper Bangkok Clay	15	3,13	4,06E-05	6,75E-03
2	Upper Bangkok Aquifer	25	2,08	1,37E+01	5,00E-04
3	Lower Bangkok Clay	30	1,04	4,65E-05	7,70E-04
4	Lower Bangkok Aquifer	60	6,25	1,37E+01	5,00E-04
5	Phra Pradang Clay	70	2,08	1,77E-06	2,12E-04
6	Phra Padang Aquifer	120	10,42	1,78E+01	5,00E-04
7	Nakorn Luang Clay	130	2,08	9,01E-07	1,67E-04
8	Nakorn Luang Aquifer	180	10,42	1,61E+01	5,00E-04
9	Nonthaburi Clay	190	2,08	7,29E-07	1,15E-04
10	Nonthaburi Aquifer	240	10,42	1,71E+01	5,00E-04
11	Sam Khok Clay	250	2,08	3,37E-07	7,72E-05
12	Sam Khok Aquifer	300	10,42	1,61E+01	5,00E-04
13	Phaya Thai Clay	310	2,08	1,40E-07	1,17E-04
14	Phaya Thai Aquifer	360	10,42	1,08E+01	5,00E-04
15	Thon Buri Clay	370	2,08	2,07E-07	5,00E-05
16	Thon Buri Aquifer	420	10,42	3,70E+00	5,00E-04
17	Pak Nam Clay	430	2,08	2,07E-07	5,00E-05
18	Pak Nam Aquifer	480	10,42	1,75E+01	5,00E-04

Summarizing all the collected data:

- Thickness and spatial distribution of Holocene sediments
- The orientation of the layers in N-S and E-W direction (as portrayed in various sketches)
- Outcropping of the major productive aquifers at the eastern and western basin flanks
- Average thickness of aquifers and aquitards
- Average hydraulic conductivity values for aquifers and aquitards

By utilizing the information, a geological model was constructed using the Python coding environment. A layer-wise calculation approach was used. The process can be simplified by following equation:

$$Bottom\ of\ layer\ x = bot_{x_{-1}} - (m * c * a) \qquad (4)$$

- $bot_{x_{-1}} = bottom\ elavation\ of\ overlaying\ layer\ [L]$
- $m = thickness\ estimation\ for\ each\ layer\ [\%]$ *based total sediment thickness (DEM-BASE)*
- $a = area\ covered\ by\ the\ layer$ (for continuous layers this equals 1 for the entire model area)

- $c = corection\ factor\ to\ account\ for\ uncontinous\ layers$

Starting with the DEM as the top elevation of the system, the raster containing spatial distribution and absolute thicknesses of Holocene sediments (bottom layer 1) was subtracted using equation 4. Following this procedure top and bottom were defined for each geological layer. Outcome is a basin structure including E-W semi horizontal layers with Holocene sediments covering the central part of the basin and 2nd to 5th layer cropping out at the basin flanks (Figure 19).

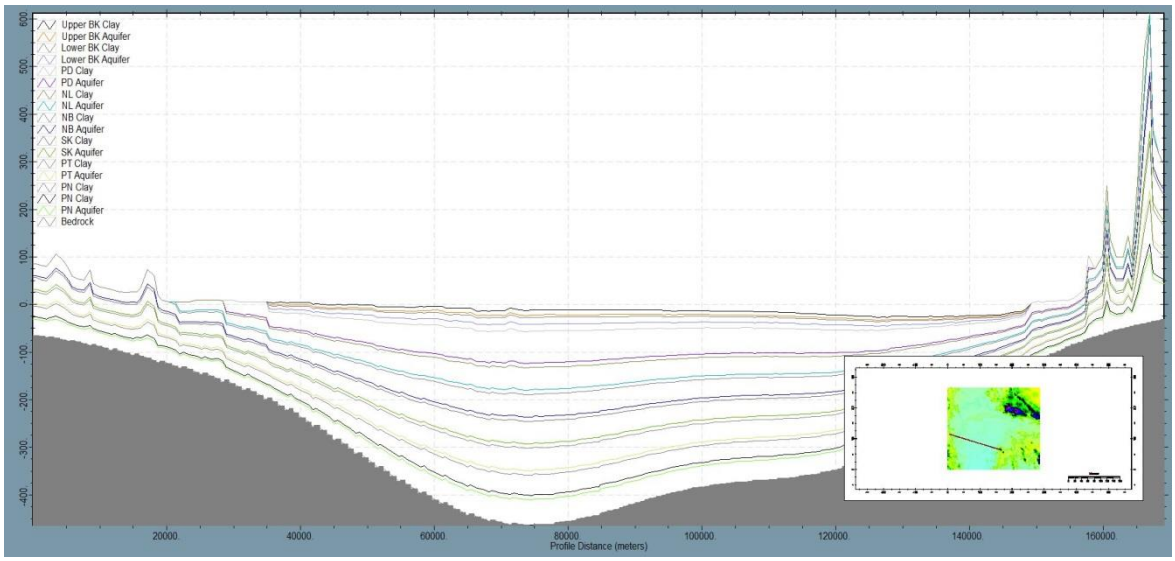

Figure 19: E-W cross section of the geological model layers showing an outcropping of the PD, NL and NB aquifers on the eastern and western basin flanks (the steep parts in the western area are inactive and can be neglected)

3.3.Model setup and configuration

All global data sets were provided in either raster or shapefile format fitting the geographical coordinate system WGS 1984. They were transformed from the geographical coordinate system WGS 1984 to the projected coordinate system WGS 1984 UTM 47 and cut to cover the exact model area. For the modelling software iMOD-SEAWAT and FloPy-SEAWAT inputs files and parameters are defined through packages containing the separate modules. Great emphasis was placed on keeping the settings for both consistent to allow for an objective comparison between 2D and 3D models. This includes the use of the exact same packages with their input files and parameters as defined for each package. For both models groundwater recharge, rivers and drains were included, whereas wells were not included in the simulation. The section below provides an introduction to the modelling software followed by an illustration of the model setup including the most important inputs and set parameters. An example SEAWAT runfile with configurations of the model parameters including the flow and solute transport packages and solver packages can be found in the appendix.

3.3.1 3D Model - iMOD-SEAWAT

The dimensional model is set up using the software iMOD-SEAWAT, an enhanced iMOD version of the SEAWAT code. IMOD-SEAWAT offers a user-friendly set up and configuration. Models are built using a runfile which makes connections to input packages as well as input files. Further, it offers the output of the model results in a Tecplot readable format which is used for post processing and visualisation. IMOD-SEAWAT requires iMOD's own raster format "IDF" as data inputs. Consequently, the datasets were converted to ESRI ASCII format and then transformed into IDF format with the help of iMOD's built in transformation function.

3.3.2 Model set up and configuration

The total lateral and horizontal extent of the model was chosen according to natural barriers. The transition zone to the upper Chao Phraya Plain marks the boundary to the North and mountain ranges bound the model domain to the east and west. The resulting grid has a dimension of 285 columns, 266 rows and 34 layers covering an area of 76 000 km^2. Cell size was set to 1000x1000 m.

Discretization: Previous studies have indicated variable-density groundwater flow to correlate with assigned layer thickness (Zamrsky, et al., 2018). Choosing a too coarse vertical discretization may lead to overestimation of the SWI process. Therefore the thickness was limited to not exceed a maximum of 20 m at any active model cell and the number of layers was chosen accordingly. This resulted in a discretization of 34 layers with variable thickness (Figure 20).

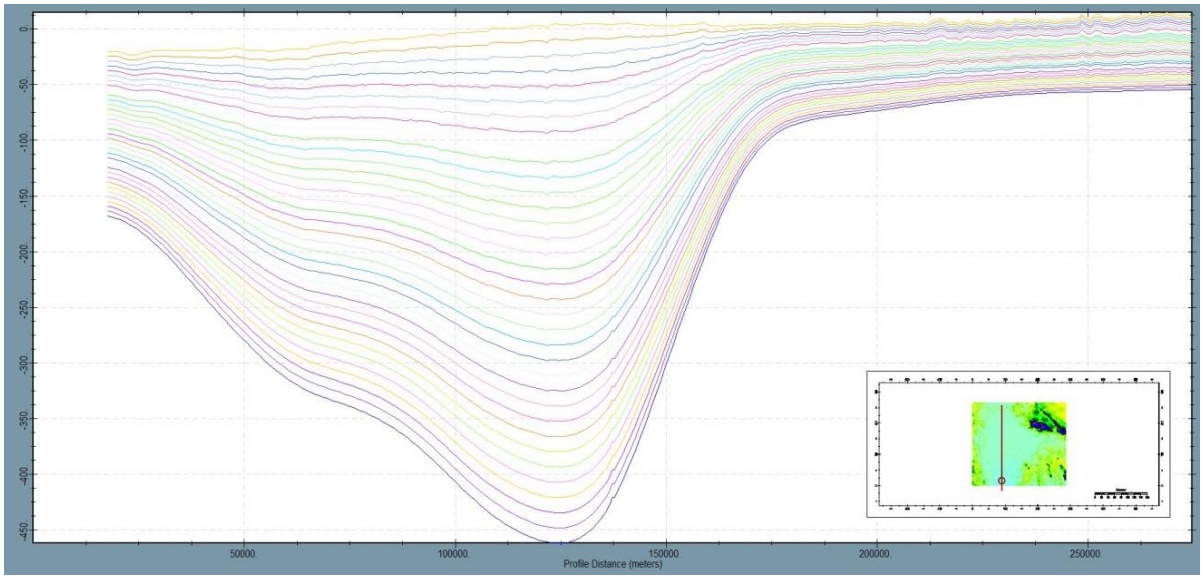

Figure 20: Model discretisation in N-S direction with the configuration of 34 layers

Boundary Condition: The objective of the model is to simulate the major hydrogeological system of the Chao Phraya Delta which is characterized by its low and even elevation. Therefore the areas with high laying mountain ranges along with the areas with consolidated geological formations mapped as the surface lithology were neglected in the simulation. Further, the steep mountain ranges bounding the Lower Central Plain create high flow velocities between neighbouring sells. This is a crucial aspect as the computational time necessary for a simulation directly depends on the maximal step size. High flow velocities greatly increase the courant number and therefore determine the maximal step size for the simulation. To allow for a faster calculation areas with extreme slopes in elevation had to be excluded. Substantial testing with different cut-off heights indicated an upper boundary at 40 m ASL to be acceptable. Following this assumption all areas with an elevation of over 40 m ASL and those with consolidated geological formations mapped as the surface lithology were set to inactive. In a classical approach the sea covered areas are set with a fixed boundary condition for concentration and hydraulic head (Figure 21). Though, previous studies have indicated the possibility of fresh groundwater in offshore areas of the continental shelf (Post, et al., 2013). Usually freshwater was stored in the sediments during times of seawater regression and afterwards sealed off by a low permeable clay layer keeping it from mixing with overlaying seawater. With Holocene Clays forming the topmost layer of the modelled system, offshore freshwater lenses are likely to be present and their possibility has to be taken into account. For this reason the boundary condition

was set to active for the entire model domain to allow for the fresh-saline interface to configure itself (see Figure 22).

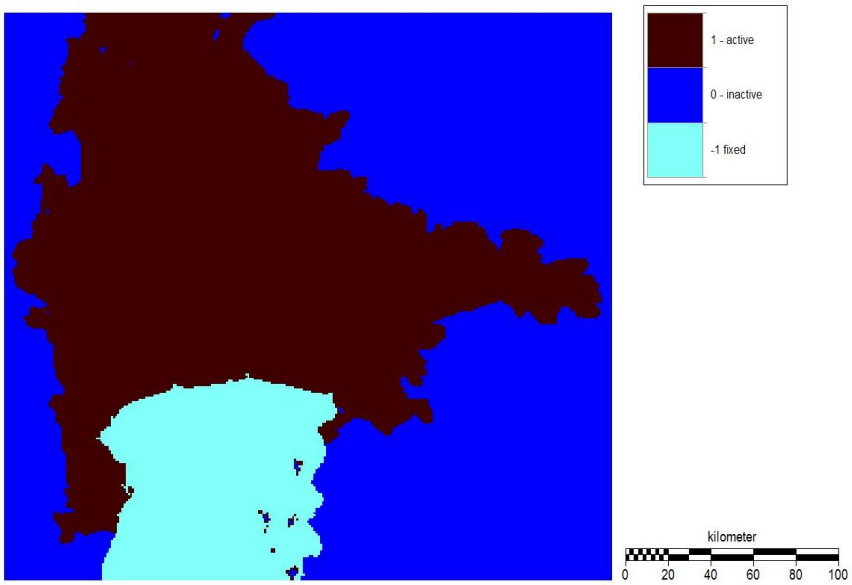

Figure 21: classical boundary conditions

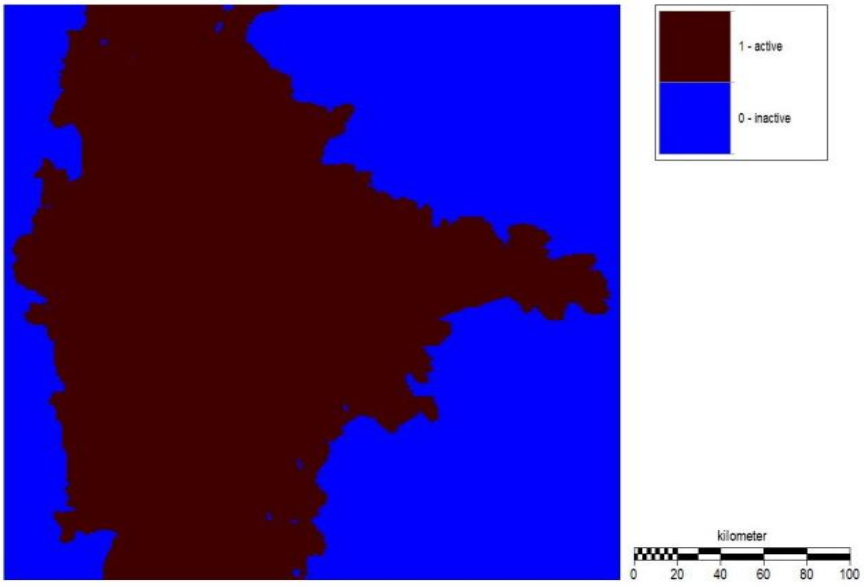

Figure 22: Paleo boundary settings

Geology: In chapter 3.2.4 a geological model was designed to include the heterogeneous local geology. Due to occurrence of inconsistent geological layers and layers of varying thickness it was not suitable as a direct input into the numerical model. Therefore a translation of geological features to the numerical model was required. The IMOD-Solid function reads hydraulic conductivity for each model cell of the geological model and assigns it to the nearest cell in the numerical model. For cases with multiple layers of the geological model inside one cell of the numerical model the algorithm averages out the value. A major downside of this algorithm is the loss of sharp translations in hydraulic conductivity between thick sand and thin clay layers. This is due to the clay layers often

being too thin to take up a complete layer in the numerical model and thus they are mixed with the sand layer, for this case resulting in conductivity values between 0.5 and 1.5 m/d. This process generated hydraulic conductivities to represent the features of the geological model. Hydraulic conductivities vary spatially for each layer but can be found in the appendix for further inspection. For the homogenous model scenario horizontal hydraulic conductivity was set to 10 m/d. The anisotropy-factor of 0.1 was used for both cases (heterogeneous and homogenous scenarios).

Rivers, Recharge, Drains: Rivers were added to the system by the use of the GAIA dataset (chapter 3.2.2). As model inputs SEAWAT requires river stage, elevation of the riverbed and river conductance. For river stage the elevation at the river cell was taken. The river bottom elevation was calculated by subtracting the river depth from elevation height (DEM) at the river location. River conductance was estimated according to section 3.2.2. Recharge was added to the top layer of the system for the land area of the model by use of the predefined raster file (section 3.2.3). Drains were set to be present 0.5 m below surface elevation with a conductance of 1000 m^2/d.

General Head Boundary: The general head boundary condition was used to regulate concentration, hydraulic head, density and conductance at certain boundary cells. The cells were placed next to the outer boundary of the model area and at the sea area for the uppermost layer. Saltwater is assumed for the ocean and therefore a density of 1025 g/L, a salt concentration of 35 g/L and a hydraulic head of 0 m ASL were assigned. Similarly the land general head boundary cells were given the density of 1000 g/L, a salt concentration of 0 g/L. The hydraulic head was set to 1 m below the elevation as a relatively high groundwater level was expected for wet tropical region. The general head boundary conductance was determined by testing for the sea and land boundary. The sea GHB was chosen according to its ability to successfully create a hydraulic head of 0 m A.S.L. for the sea covered area, while the land GHB cells were set to very low values to avoid high slopes between neighbouring GHB boundary cells and to allow for a smooth hydraulic head interface. A conductance of 0.1 for the land boundary and 10^7 m2/d for the sea boundary have proven to be suitable.

3.3.3 2D Model – FloPy-SEAWAT

FloPy is a Python package developed by a team of well-known MODFLOW users that enables to run MODFLOW, MT3D, SEAWAT and other MODFLOW related groundwater simulations by using predefined Python libraries (Bakker, et al., 2016). A major advantage is a fast and easily adjustable model setup, model reproducibility, as well as post processing including visualisation of the outcome all inside of the Python environment. Various 2D models were set up along the coastline using a script provided by Daniel Zamrsky (Figure 23). It generates perpendicular cross sections every 5 km along the coastline. The cross sections are defined to laterally span up to 200 km in both directions from the coastline. Though, this is often not the case as the length is limited by the model boundary (Figure 20). The raster input files used to construct the 3D iMOD-SEAWAT model were utilized to generate the 2D grid data for each profile. This includes the model boundary, model discretization, hydraulic conductivities, rivers, recharge, drains and general head boundary conditions. A developed Python script extracts the exact value of the 3D model input raster file and stores them in NumPy directories, which were read into the FloPy models. Each 2D model is identified by a specific id number in the format of 882xx. Dimensions for the 2D models consist of 34 layers, 1 row and x-amount of columns, depending on the lateral extent of the model. The longest 2D models are 88270 and 88267 with a length of 235.5 km and 237.0 km, or 2355 columns and 2370 columns respectively. The shortest is 8887 with 23 km length. Model 88267 expands from the northern edge of the model

domain to the southern part in the Gulf of Thailand and provides a representable coverage of the Chao Phraya River basin. It was therefore chosen for detailed analysis in the following chapters.

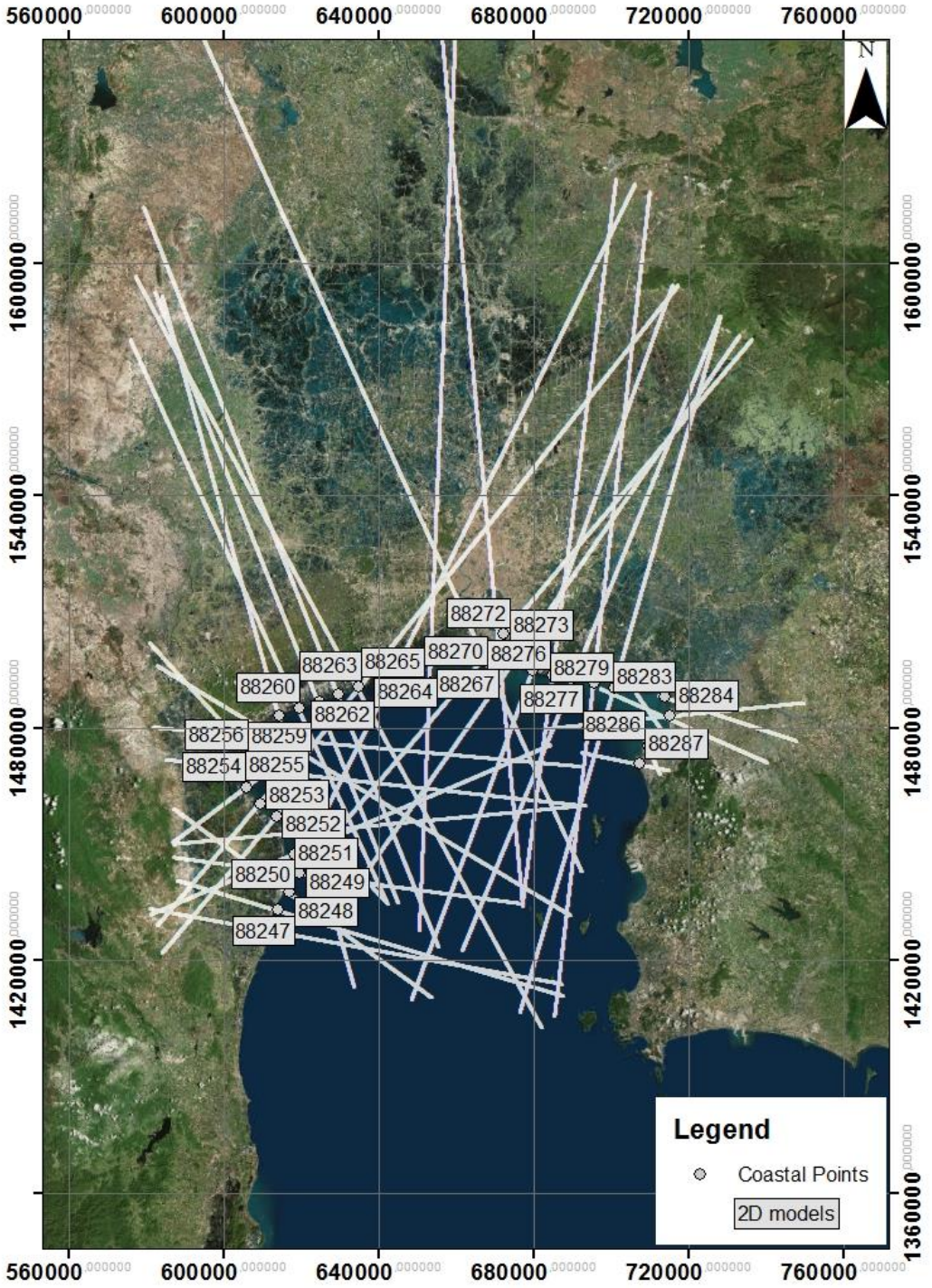

Figure 23: 2D models covering the study area

3.4 2D -3D Interpolation

In order to enable a quantitative comparison between 2D and 3D models equal model dimensions are required (including cell size and total model extent). For this purpose, the 2D model outputs were spatially interpolated to inherit the 3D cell size and to cover the 3D model domain. This was implemented using the Python programming environment. During the interpolation procedure each

2D model cell was treated separately as an observation point and consequentially stored in data arrays. These comprise of x and y-coordinates, elevation, hydraulic head, salt concentration and average flow velocities. A grid matching the dimensions of the 3D model, hence 266 rows, 285 columns and 34 layers was created and UTM coordinates were assigned. In case of the hydraulic heads the Python package Scipy was used. It offers an interpolation method simply picking the nearest observation point value to the grid cell. To even out sharp differences in hydraulic head the results were smoothed with a two dimensional spline. Results of this process are visualized in chapter 4.1.3 and following. The objective for the interpolation of the salt concentration values was to keep the fresh saline interfaces as generated by the 2D models, and not to artificially extend the mixing zone through the interpolation algorithm. Due to the highly non-normal distribution of salt concentration values (either near 0 g/L for freshwater or around 35 g/L for seawater with a thin transition zone containing the spectrum of values in between) a log transformation was applied to approximately conform to normality. Afterwards, ordinary kriging was performed by utilization of the PyKrige toolbox (https://github.com/bsmurphy/PyKrige). The evaluation of the variogram function and the lags are produced internally inside the kriging algorithm. Comparison of the results showed a better reproduction of the salt concentration values by the much faster nearest method. This can be attributed to the extremely high density of 2D models in the area of transitioning salt concentration (right in the Bay of Thailand and near the shoreline). Additionally, the 2D models are orthogonally oriented to the coastline, which supports the concept of a nearest interpolation as the isoclines of equal salt concentration are typically parallel to the coastline. Taking in the computational demand to calculate the interpolation for all scenarios the nearest method has proven to be much more efficient and was used to also interpolate salt concentration values. It should be noted, the 2D-3D interpolation is solely used for the freshwater volume calculation. Analysis of salinization patterns was evaluated through the use of representative 2D cross sections due to illustrative benefits.

4. Results

The simulation results of the 2D and 3D model scenarios as well as its consecutive 2D3D interpolation are displayed and analysed in the following chapters.

4.1 3D Models

4.1.1 Model scenario 3D_A

A three dimensional geologically homogenous sand model was constructed to verify flow behaviour and general model settings (3D_A). Additionally, it was used to compare 2D and 3D in a homogenous setting. Simulation results for 10 kyrs are shown below in Figure 24. Hydraulic heads generally follow the elevation. In the offshore area the general head boundary effectively forces the hydraulic heads to 0 m AMSL. A fast salinization of the Bangkok Bay can be observed. Salt water intrusion continues to progress further inland even after ten thousand year meaning that equilibrium between fresh and saltwater could not be reached. Slices along the y-axis reveal continuous spreading of the mixing zone between 5 and 10 kyrs. The mixing zone is not homogenous as would be expected for a homogenous setting. Vertically upwelling salinization patterns can be observed (Figure 24).

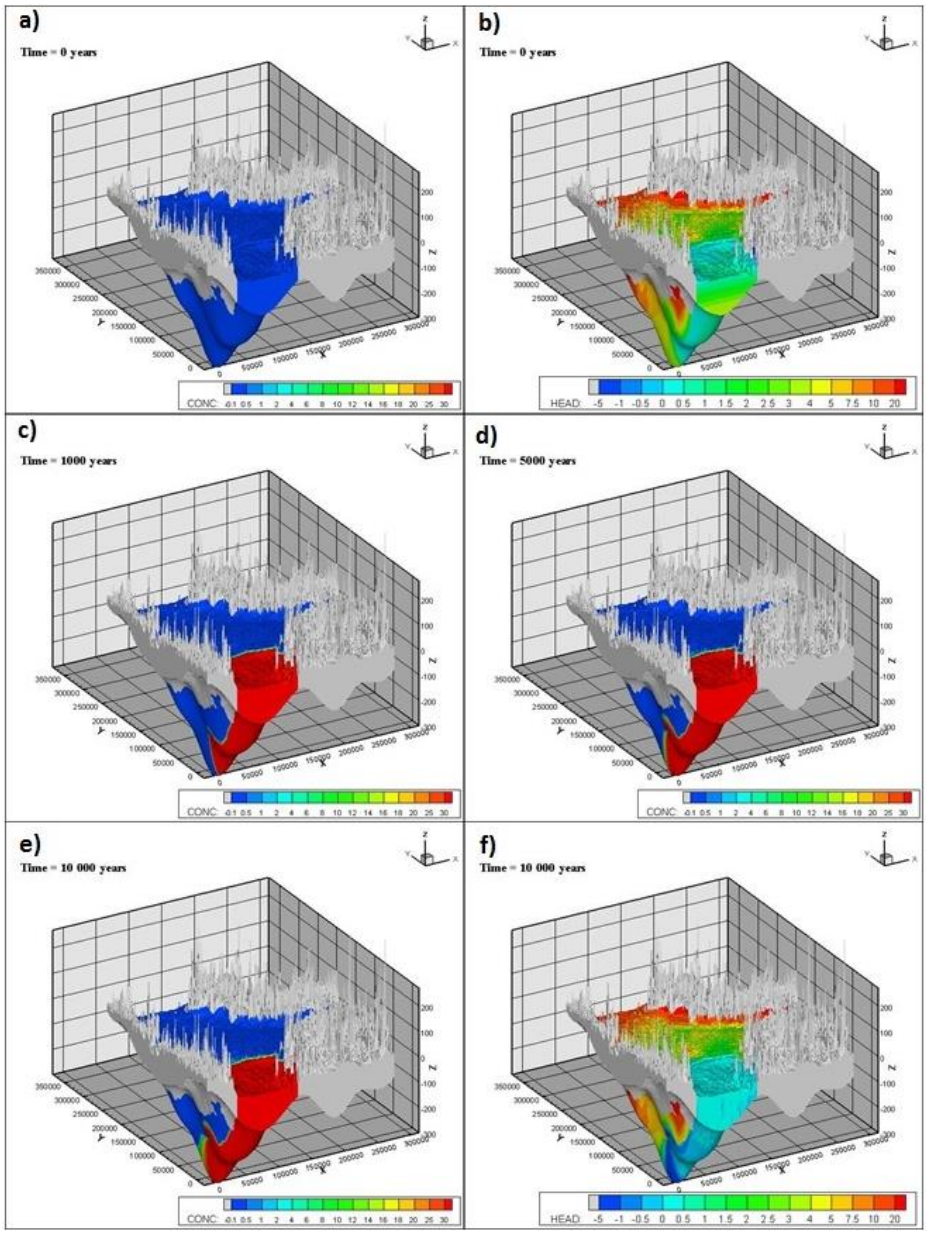

Figure 24: homogenous 3D model (3D_A) a) initial starting salt concentrations; b) initial starting hydraulic head; c) salt concentration after 1000 years; d) salt concentration after 5000 years; e) and f) salt concentration and hydraulic head after 10 000 years

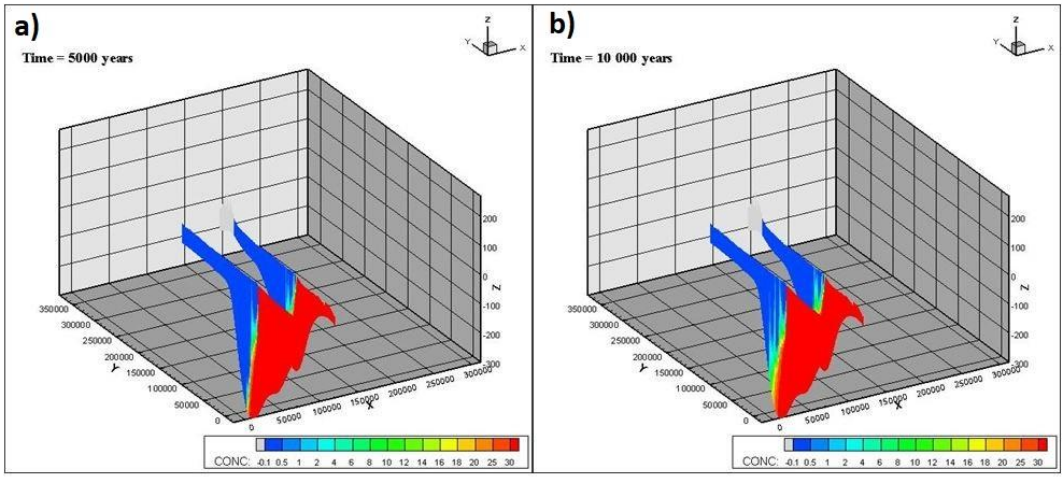

Figure 25: 3D_A 2D slices showing vertical salinization patterns a) after 5000 years; b) after 10 000 years

4.1.2 Model scenario 3D_B

An almost identical model configuration as in 3D_A was used to set up the next model scenario 3D_B, the only change being the implementation of hydrological properties based on the geological model developed earlier. For the deeper aquifers, salinization appears to be very similar to the homogenous model. This can be accounted to the presence of thick aquifers dominated by sand and gravel with similar hydrogeological properties as in 3D_A. Saline water quickly penetrates into these areas and migrates towards the upper layers with an upward flow. The observed salinization behaviour can be attributed to the inflow of saline seawater generated by the general head boundary cells at the seaward model boundary. The upper layers reveal quite significant differences in salinization patterns. Some areas in the western part, but predominantly the eastern part of the Gulf area show fresh water to be present in the top layers (Figure 26). Fresh water stays prevalent even after the majority of the system has salinized as it is stuck beneath the clay layer, floating above heavier seawater.

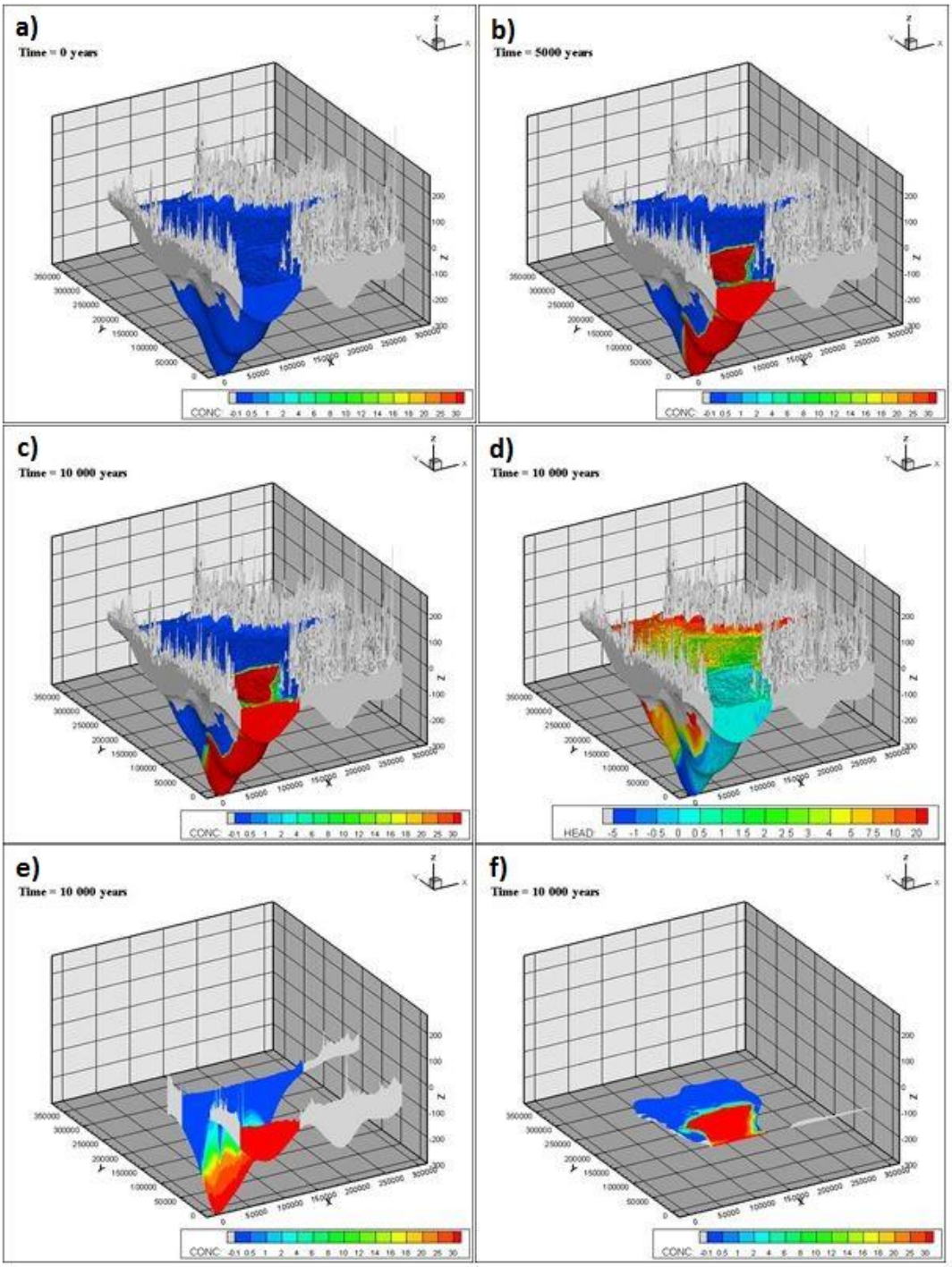

Figure 26: Model 3D_B a) intial concentration b) concentration after 5kyrs c) concentration after 10kyrs d) hydraulic heads after 10kyrs e) slices orthogonal to the y-axis f) slice orthogonal to the z-axis at depth of 300 m

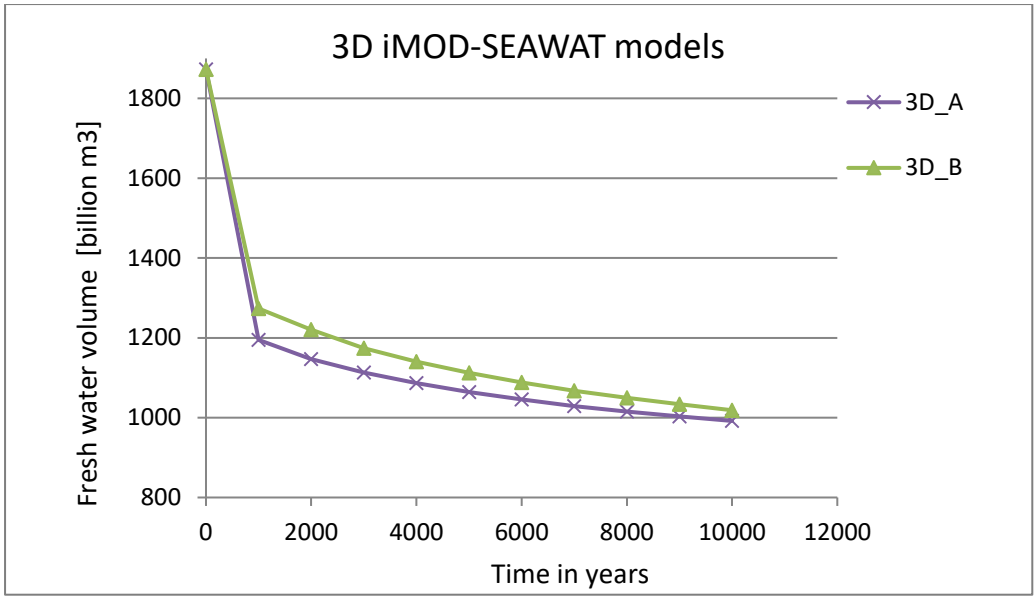

Figure 27: Fresh water volume over time for 3D_A and 3D_B

Comparison of total freshwater volume confirms the above explained observations and indicates that more fresh water is present in the heterogeneous setting (Figure 27). However, the differences in estimated freshwater volumes seem to gradually decrease over time (Figure 28). This may be explained by the salt-fresh distribution in the homogenous model reaching near equilibrium state relatively quickly. While the heterogeneous case on the other hand requires much longer durations to reach an equilibrium state. The effects of dispersion in the heterogeneous setting are also likely to account to this difference.

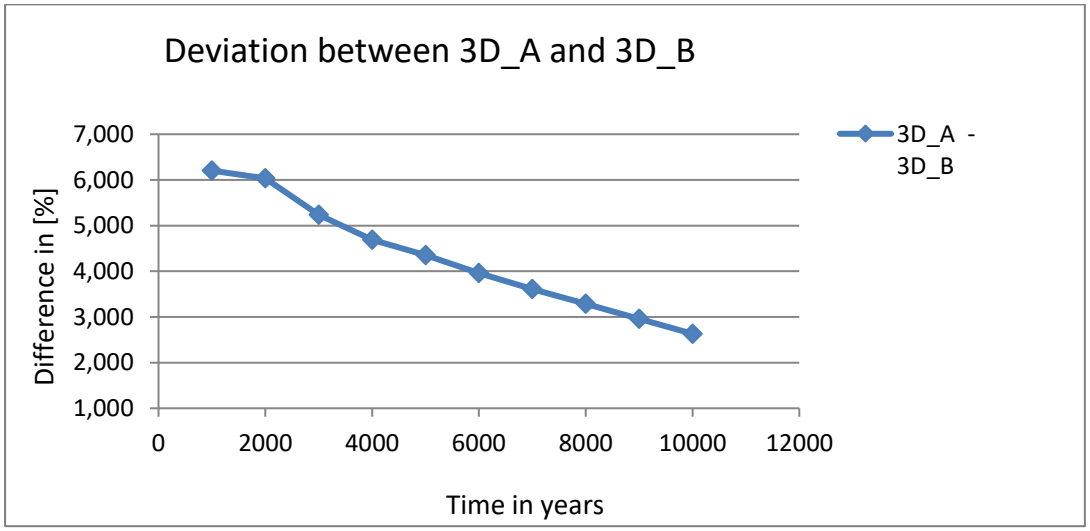

Figure 28: Development of fresh water volume over time

4.2. 2D Models

Following section displays 2D model results for the homogenous scenario (2D_A) and the heterogeneous scenario (2D_B).

4.1.3 Model scenarios 2D_A and 2D_B

Figure 29 shows all 35 homogenous 2D SEAWAT models plotted in the study area. Initially the 2D models are designed to be oriented exactly perpendicular to the coastline. Notches and little bays generate small variations of the coastline. Following this, the 2D models occur in multiple angles, some in very small angles to the general sea-land contact. As a result, each model is crossed by multiple other models and the high density of 2D models provides a good coverage of the study area. Distribution of hydraulic heads and salt concentration reveals the course of the coastline and the general shape of the Bangkok bay is clearly visible. As each 2D model is calculated separately they may have significantly different values at neighbouring cell locations of an opposing 2D model. The 2D models were run for a homogenous (Figure 29 a/b) and heterogeneous setting (Figure 29 c/d) with identical hydraulic properties as the 3D model. Both 2D model configurations seem to yield similar results to those seen in the 3D model for the majority of the model domain.

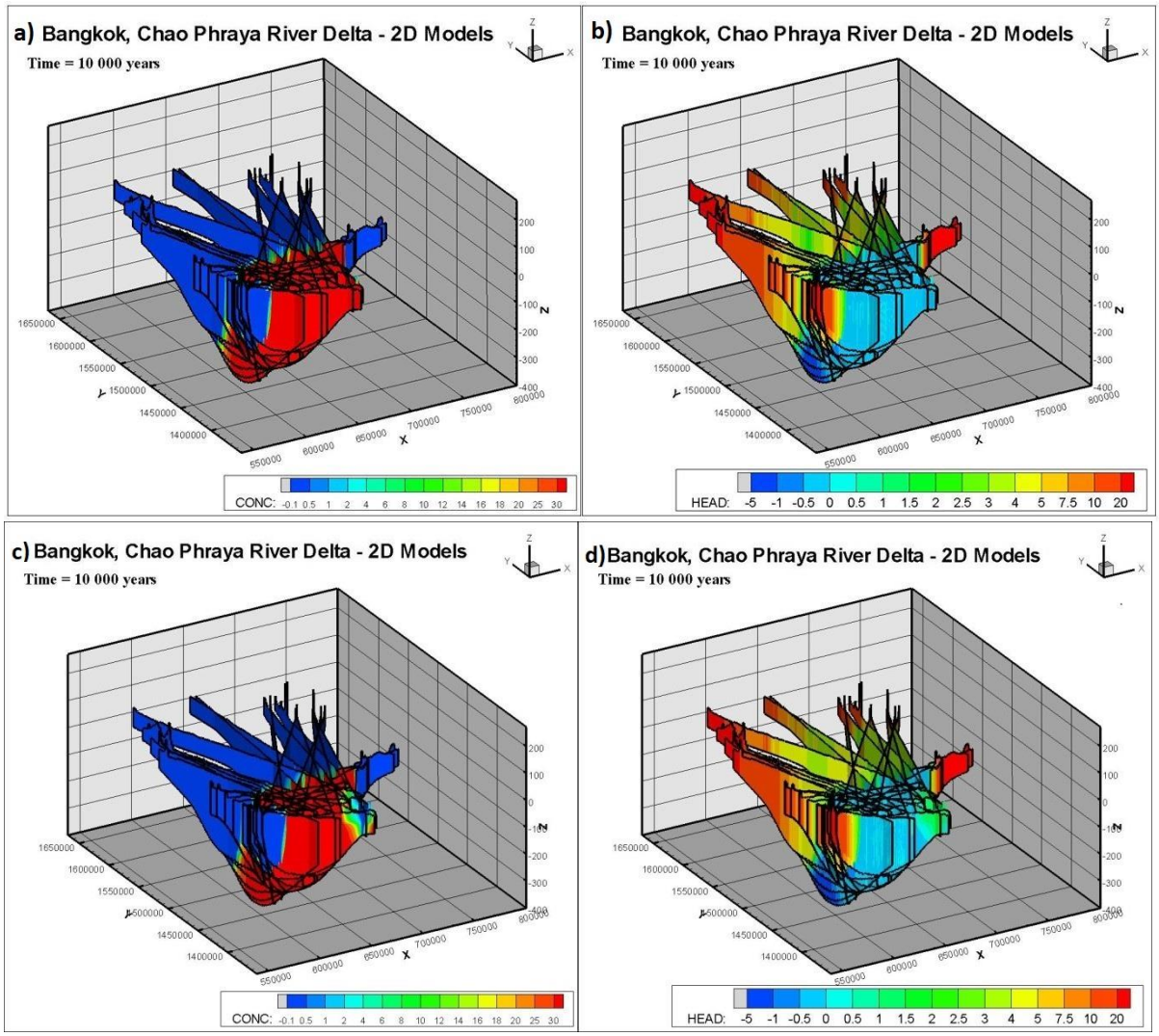

Figure 29: 2D models covering the delta a) 2D_A: salt concentration after 10 kyrs; b) 2D_B: hydraulic heads after 10 kyrs; c) 2D_B: salt concentration after 10kyrs; 2D_B: hydraulic heads after 10kyrs

4.3.2D vs 3D Comparison

Following sections provide a detailed presentation of the 2D and 3D results and more precisely their comparison in terms of fresh water volume, salinization pattern, and computational demand. Furthermore, the influence of rivers on both 2D and 3D models is illustrated along with a 2D model density analysis.

4.3.1 2D-3D Interpolation

All 2D models were spatially interpolated to fit the grid of the 3D model (Figure 30). Model scenario 3D2D_A represents the interpolated 2D sand models and model 3D2D_B the version with implemented local geology. At a first glance, the 2D3D models seem to reproduce the 3D model results quite well. For both models the distribution of hydraulic heads and salt concentration seem plausible and don't reveal any conspicuous areas deviating far from the expected values. The heterogeneous setting 3D2D_B shows less salinization in the upper layers. Freshwater is present in the eastern part of the bay area, coinciding with the 3D model results. Detailed evaluation of the area with prevalent freshwater indicates a slight difference between the interpolated 2D3D model and the initial 3D model for the heterogeneous setting. It seems as more salinization has occurred in the 2D models. The 3D_B model shows fresh water in the shallow aquifers in the western part of the bay, which cannot be found in the interpolated 2D version of the same scenario. Furthermore, the freshwater prevalent in the aquifers of eastern part of the bay covers far less area than for instance in the 3D_B model.

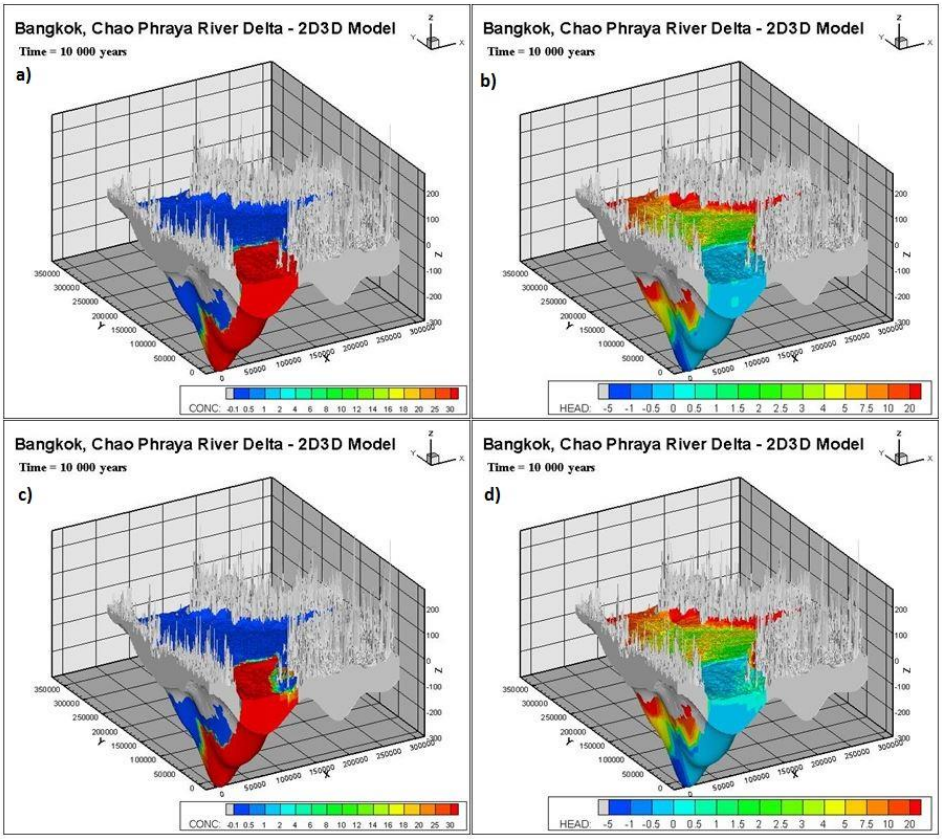

Figure 30: 2D-3D interpolation results a) 3D2D_A salt concentration b) 2D3D_A hydraulic heads c) 2D3D_B salt concentration d) 2D3D_B hydraulic heads

4.3.2 Fresh water volumes and salinization pattern

In terms of total freshwater volume, the 3D model scenarios contain more freshwater than equivalent 2D3D model scenarios. For both scenarios in 2D and 3D the differences between geological settings A and B decreases over time (Figure 31). The difference between interpolated 2D and initial 3D model for the homogenous setting is quite small, deviation accounts to only 0.3 % to 0.5 % and appears to be constant over time. This is not the case for the heterogeneous setting. Instead the deviation is measured between 4.5 % after 2 kyrs of runtime and decreased down to less than 2 % for 10 kyrs. This supports observed differences between Figure 26 and 30. Furthermore, it can be noticed that the deviation between model scenarios 3D_A and 3D_B is quite significantly larger than that of the same configuration of the 2D interpolation.

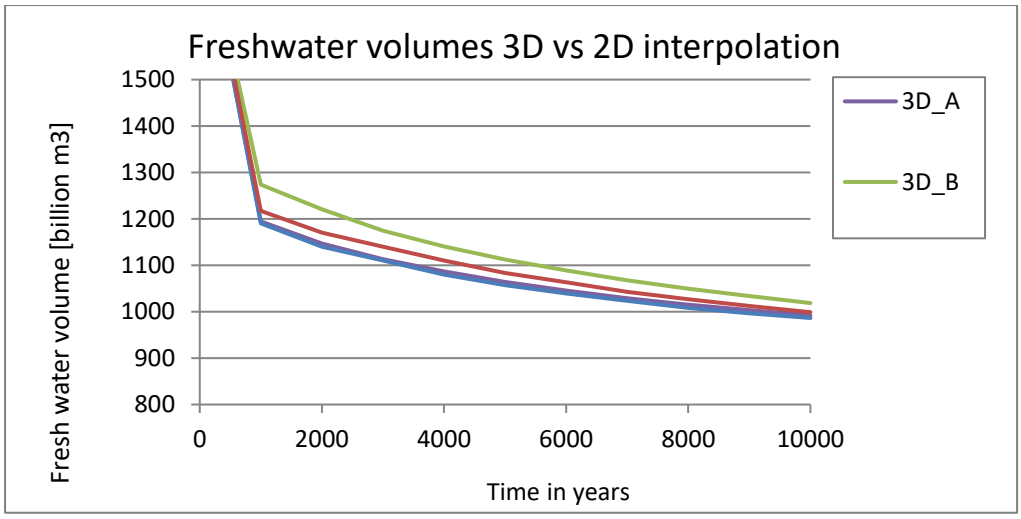

Figure 31: Freshwater volumes 2D vs 3D

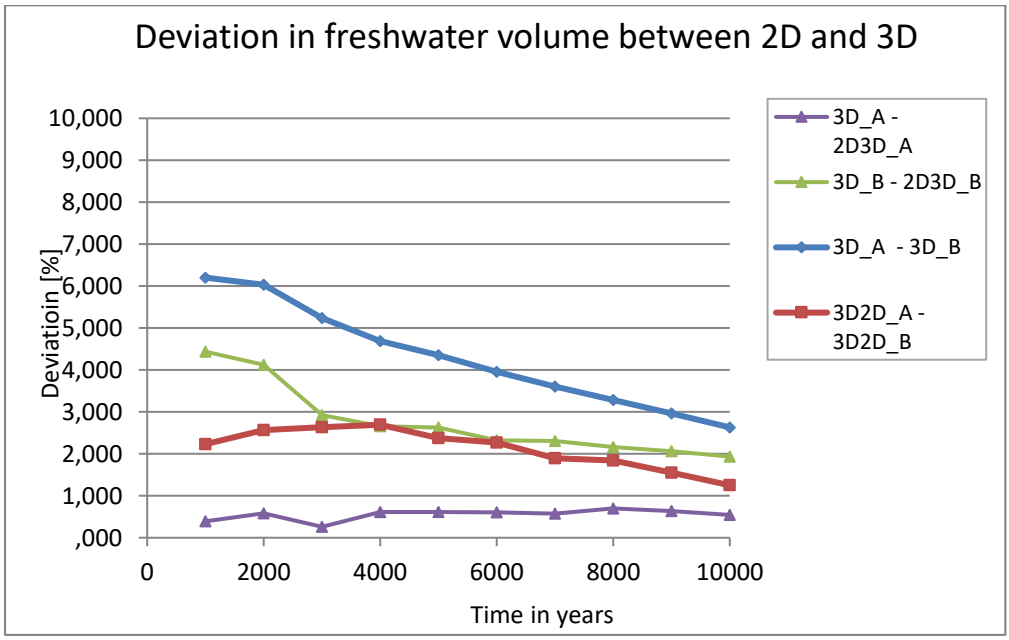

Figure 32: Deviation between model types

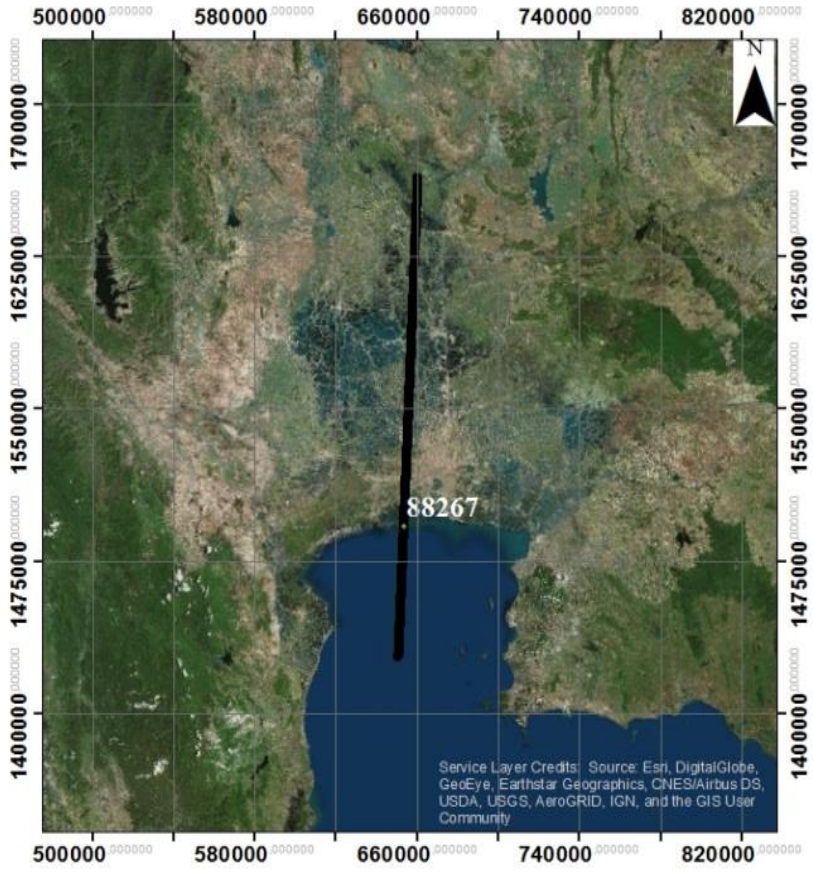

Figure 33: Representative cross section 88267 (WGS 1984 UTM Zone 47N)

Salinization patterns at the location of cross sections 88267 were analysed in detail for the 3D_B model scenario and its equivalent 2D version. Profile 88267 was chosen due to its North to South coverage of the delta. Figure 34 c shows the subtraction of the mentioned two model scenarios for cross section 88267. There seem to be differences in the salinization patterns between 2D and 3D. For the 2D model scenario, salinization rate increases towards the coastline in the top of the saltwater-freshwater contact zone. Differences in salinities range up to 20 g/L and are spread out over a distance of 2.5 km.

In the deeper parts of the system a more spread out deviation can be observed. Deeper areas reveal the 3D model to have a more widely spread out mixing zone with values 0.5 to 2.5 g/L higher in salinity. But contrary an area inside of that mixing zone is then again more saline for the 2D model. Potentially the unstable character of variable-density groundwater flow results in a slight discordance for the deeper aquifers. The 2D model shows a generally further progressed salinization. A greater numerical dispersion could account to the wider mixing zone as seen in the 3D model. A greater numerical dispersion can be initiated by the difference in cell size length of 1 km for 3D models and 100 m for 2D models.

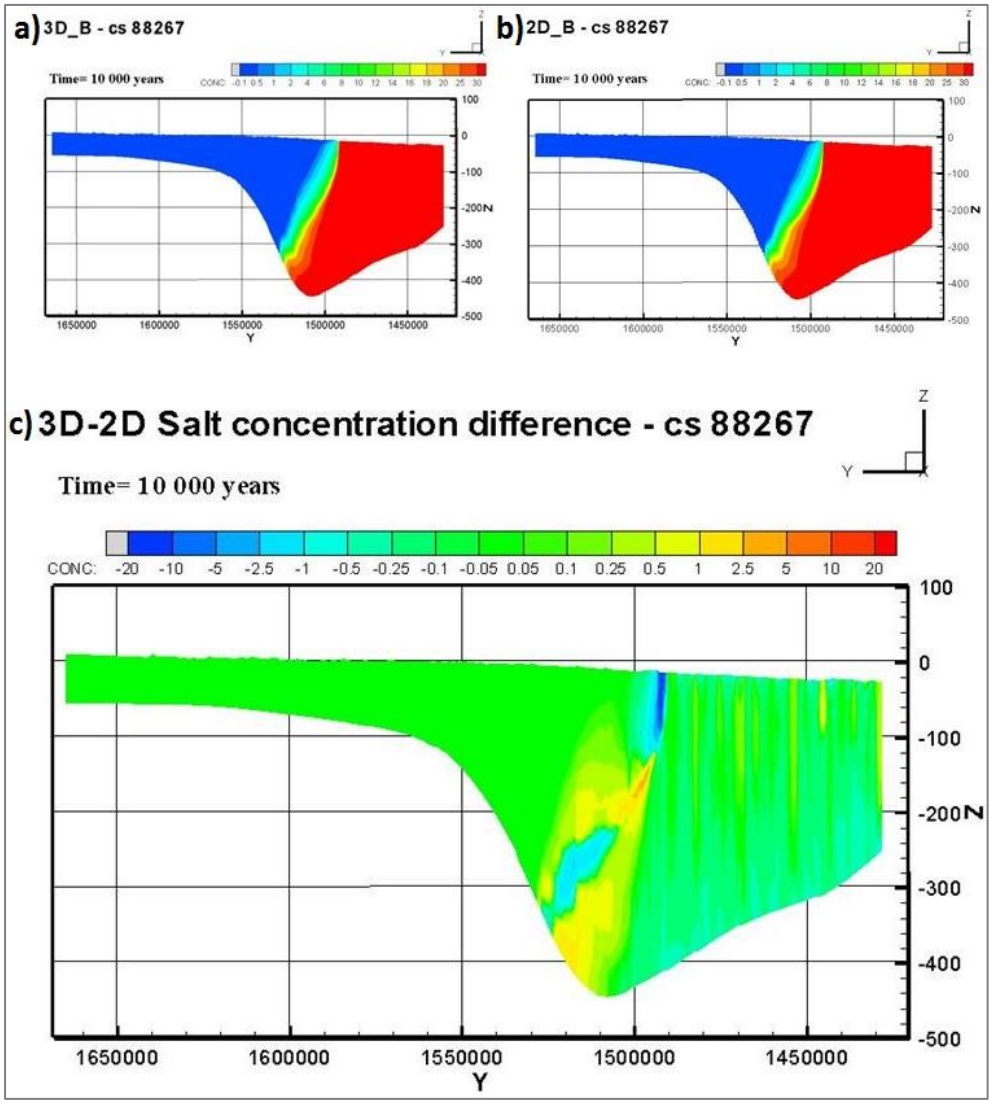

Figure 34: Cross section 88267 produced by a) 2D and b) 3D variable-density groundwater models c) 3D minus 2D salt concentration for cross section 88267

Table 4: Quantitative results for the modelling scenarios

Model	Fresh ground water volume [10^9 m3]	Solute (mass) [10^9 kg TDS]
3D_A	991.8	26616.6
3D_B	1018.6	24637.7
2D3D_A	986.4	27841.0
2D3D_B	998.9	27191.1
3D_B_R1	1014.1	24819.4
3D_B_R2	1024.9	24437.5
2D3D_R1	1002.0	25580.5
2D3D_R2	1000.6	25479.8

4.3.3 Density of 2D models along the coastline

The freshwater volumes demonstrate relatively good correlations of 2 to 4.5 % for 2D and 3D model scenarios. Nevertheless, it is very unlikely for studies to use such a high amount of cross sections to cover such a large scale coastal groundwater system. Therefore a 2D model density analysis was conducted to understand the required amount of 2D covering a deltaic area. Offsets between cross sections perpendicular to the coast were tested for 5k, 10km, 20km and 40km and afterwards interpolated to cover the 3D model domain. It was expected for the interpolations with a greater offset of 2D models to perform worse than those with a closer coastal model interval. Surprisingly, the interpolation with the least amount of cross sections covering the delta managed to resemble the freshwater volume of the initial 3D model the best (Figure 35).

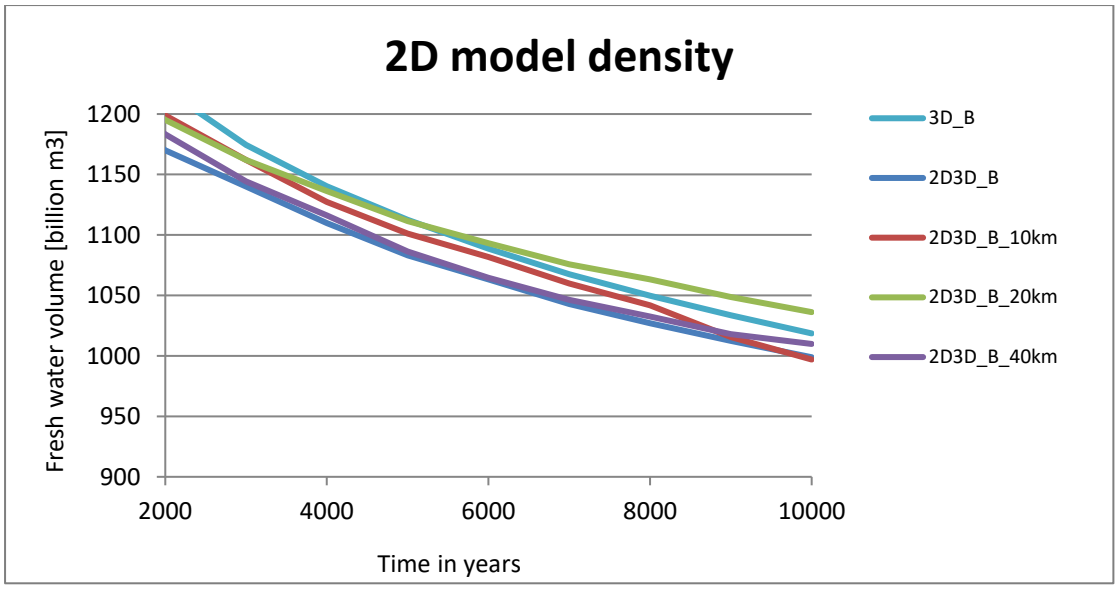

Figure 35: 2D3D interpolation with varying offset of 2D models

4.3.4 Computational demand

For many projects and real life applications computational time is a relevant factor in terms of modelling choices. Calculation times were measured for 2D and 3D model scenarios. Average computational time of 2D models for 10 000 years ranged between 8 minutes and 2 hours. In comparison computational time necessary to simulate the same runtime for the 3D model ranged between 40 and 60 hours depending on model configuration. A direct comparison of computational demand between 2D and 3D models does not result in a meaningful exemplification as they represent different dimensions and model domain sizes. But to give an illustration about computing time we compared the sum of computation time of all 2D model scenarios with that of the 3D model scenarios (Figure 36). Another advantage of two-dimensional models is low requirements of computational memory, which allows for simultaneous computation of multiple models on the same device. This is not the case for the 3D model as random-access-memory is maxed out relatively fast. For example, to run a 3D model with identical grid size, resolution and model inputs as the case in this project with the simple addition of multiple changing general head boundary conditions would require RAM of over 8 GB. The use of a specialized high memory computational device would be required.

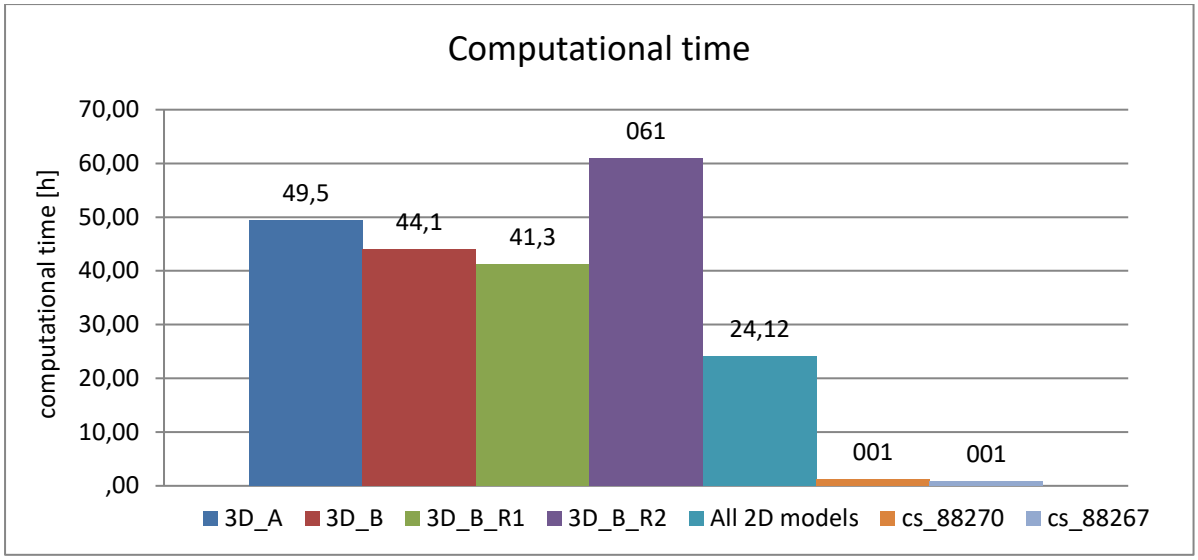

Figure 36: Computational time for the modelling scenarios

4.3.5 2D_B extended simulation time

The representative 2D model 88267 was run for a duration of 150 thousand years to obtain a sense of the fresh-saline distribution present in the system over a longer time period. Inspection of the results reveals a continous saltwater intrusion forming a wedge under the buyount freshwater. The arrow in Figure 37 indicates the shoreline, consequently, the areas to the right are below sea level. According to this cross section freshwater continues to be present in the offshore area even after a duration of 150 kyrs.

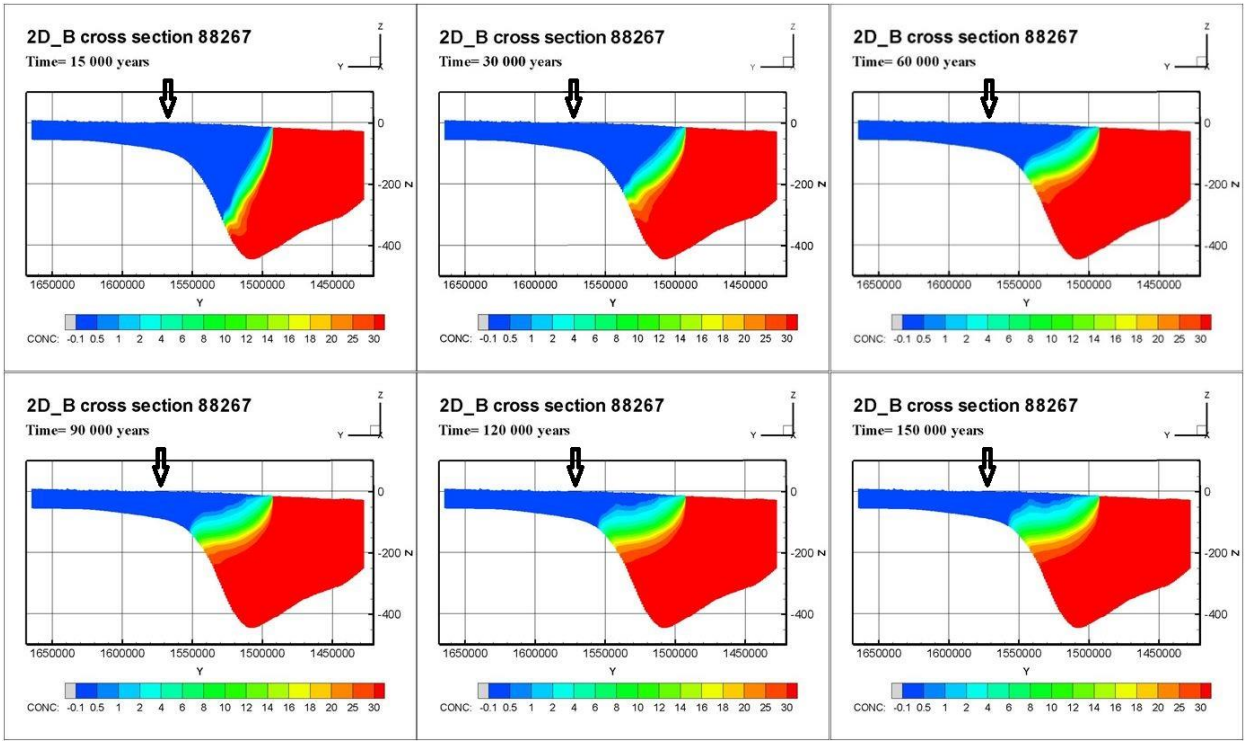

Figure 37: Salt concentration of cross section 88267 after 15 - 150 kyrs

4.3.6 River Sensitivity Analysis

Since rivers play an important role in the surface-groundwater flow interaction, the impacts of river systems on the results of the 2D and 3D variable-density groundwater flow model scenarios were analysed. In order to do that, the river conductance was modified to observe behavioural changes in both model types. For scenario R1 river conductance was reduced to half of its initial value and doubled for scenario R2. The 3D model shows noticeable impacts in the flow regime around the river locations. Interactions between rivers and the groundwater system are indicated by the presence of high flow velocities forming cone like variations in the velocity field. Rivers can provide recharge to the groundwater systems through infiltration, especially when the river stage is above the groundwater level. On the other side, they can act as draining water bodies if the opposite situation occurs. Upward flow velocities indicate draining river bodies (yellow and red cones). Rivers suppling groundwater recharge can be observed by increased downward velocities (blue cones). This can be observed in Figure 38. Rivers for scenario R1 reach up to 15 to 20 m downward into the aquifer. For the case of the scenario R2 the influences of rivers can be observed for depths up to 30 to 35 m into the aquifers.

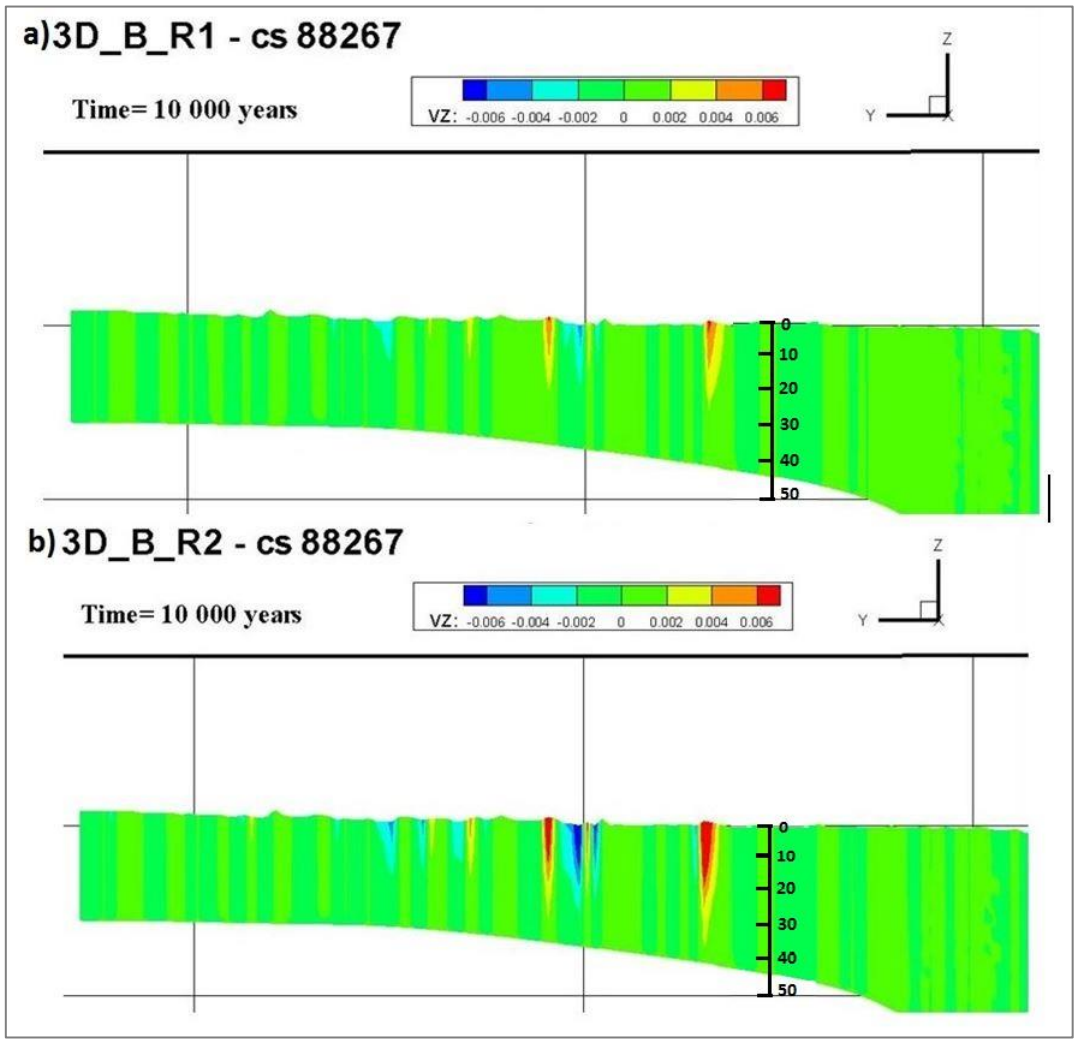

Figure 38: Cross section 88267 extracted from the 3D model showing flow velocities in z-direction in m/d.

As expected, the influence of the rivers increases with higher river conductance. In case of the 3D model a near linear relationship can be observed (Figure 39). The correlation between more freshwater being present with a higher river conductance indicates that rivers supplying groundwater to the system outweigh those which drain groundwater out of the system. As a result, increased hydraulic heads can be expected, which thereby act as a higher opposing force to intruding variable-density groundwater flow. The 2D models with the same river conductance do not reproduce the results seen in the 3D model.

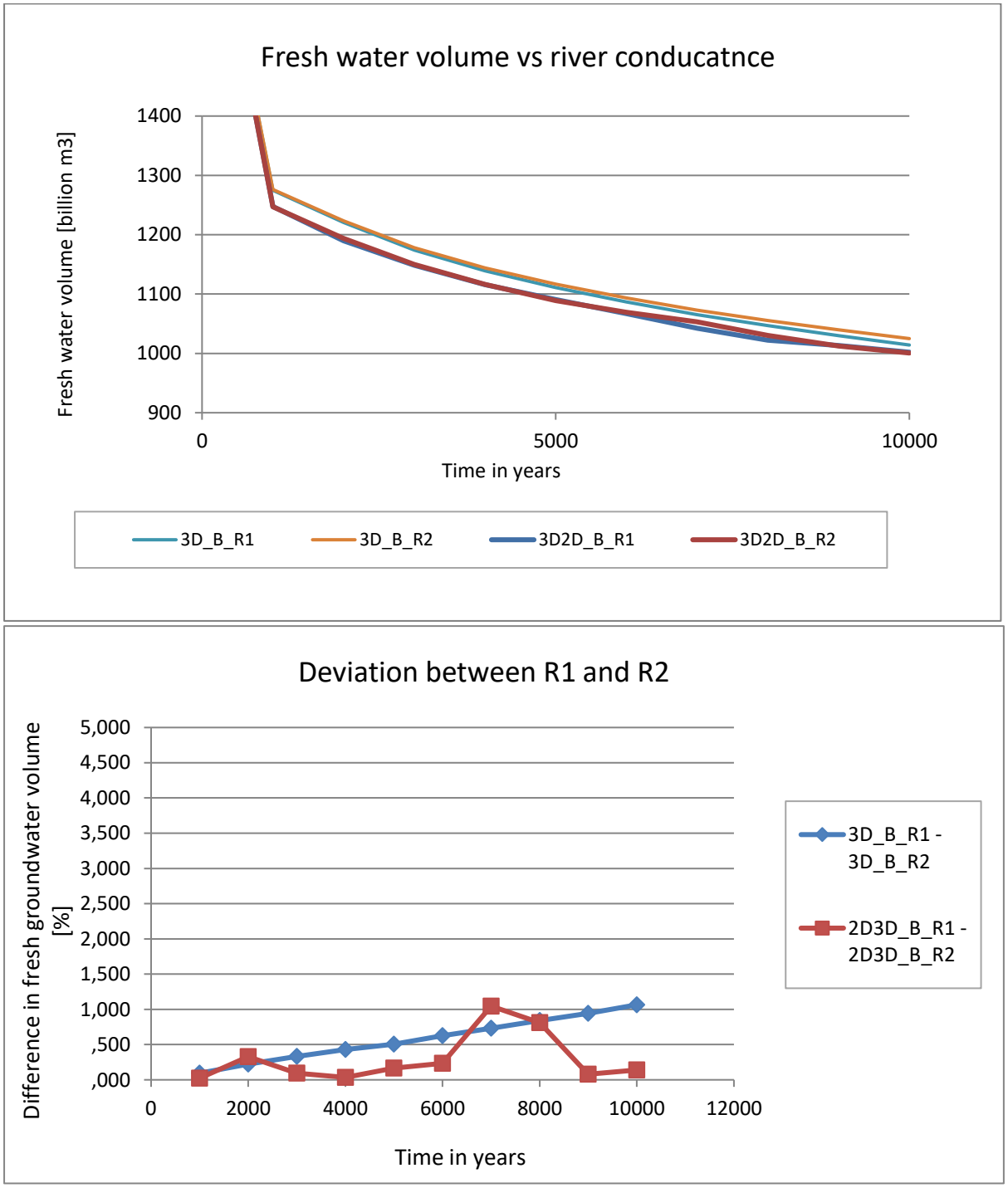

Figure 39: a) Total freshwater volume for river scenarios b) deviation between river scenarios for 3D and 2D3D models

The influence of river conductance on freshwater quantity increases over time for the 3D model scenarios. Slight changes in other model parameters seem insignificant at first, but when the model

reaches a halfway stable configuration between fresh and salt the impacts of these changes become visible. Observation of the flow velocities for the 2D models reveals substantial differences. The river systems seem to have far less influence on the groundwater system. For scenario R1 local variations of flow velocities are hardly visible. For scenario R2 an increased influence can be identified, but it is significantly less than previously documented in the 3D model. Inspecting the cone shaped variations of flow velocities reveals that the interaction between certain river cells may be different for the 2D model and 3D model. A river which primarily acts as a water draining body in the 3D model is observed to act as water supplying in the 2D model and vice versa. To identify whether the rivers are the cause of the volume difference between 2D and 3D models both were run without the river package being activated. The results show the deviation between 2D and 3D to stay constant at 2 % with deactivated river package. Compared to the initial offset of 2D3D and 3D model this is not an improvement.

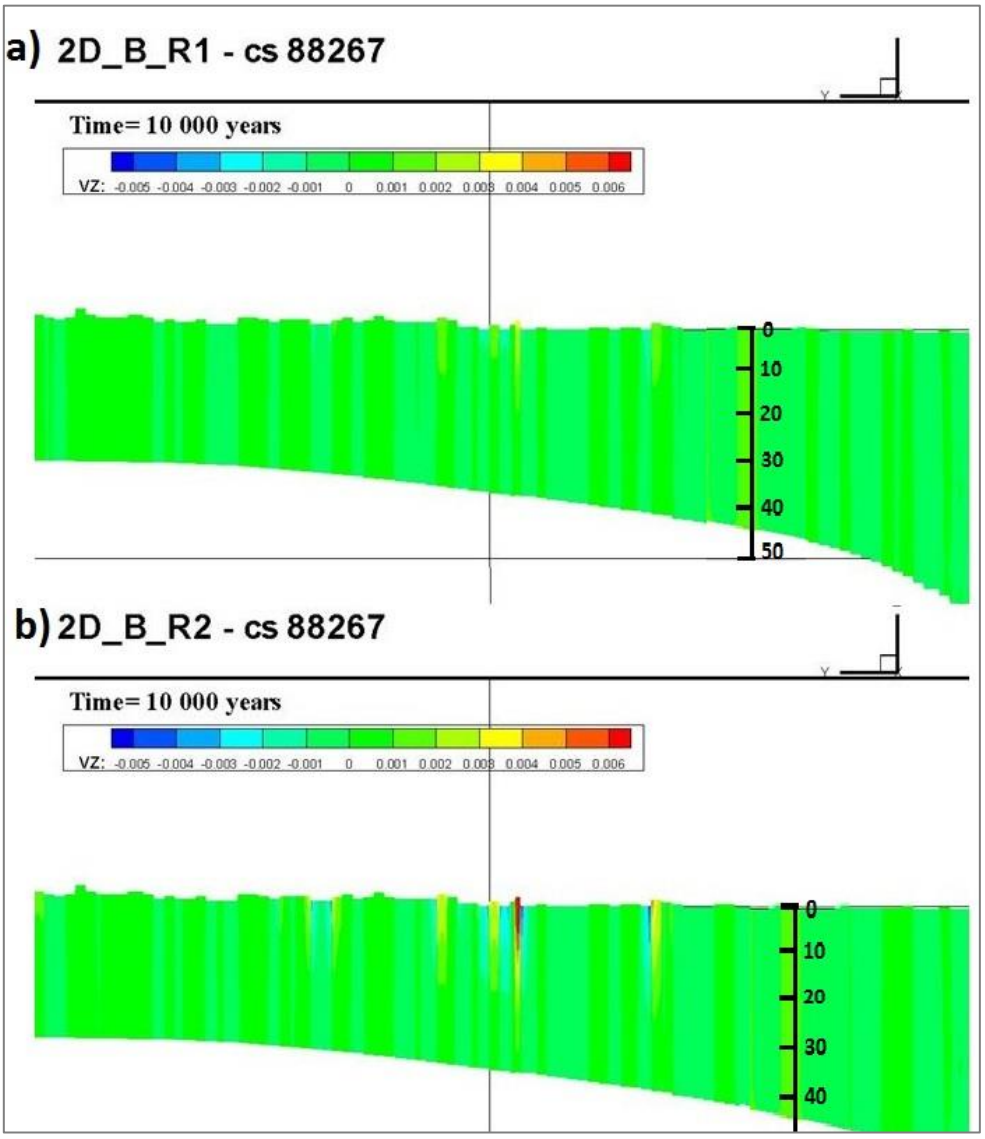

Figure 40: Cross section 88267 showing flow velocities in z-direction in m/d for river scenario a) R1 and b) R2

5. Discussion

In this chapter the modelling results are discussed in context of the research questions as defined in chapter 1.2.1. Research question 1 and 2 are highly interconnected. Out of this reason the 1st and 2nd research questions are addressed jointly in the first paragraph.

1. *How do 2D and 3D models quantitatively compare in regard to fresh groundwater quantity and salt distribution pattern? 2. How does the implementation of local geology impact the applicability of 2D and 3D models?*

The results show the 3D model scenarios contain more freshwater than equivalent 2D scenarios. The differences between 2D and 3D are considerably low when the total amount of fresh groundwater is considered: e.g. with 0.5 % offset for the homogenous case. This coincides well with the observations made in previous studies. Knorr et al (2016) has also illustrated a good correlation between 2D and 3D in a homogenous setting through the reproduction of sand column experiments by 2D and 3D numerical models. The results in this study indicate the reproduction of 3D systems through 2D models to also be applicable for large spatial scales under the condition of homogenous material. The slight mismatch of 0.5 % could potentially be accounted to errors in the interpolation procedure, and the size of the area under consideration. Further testing with an increased amount of 2D cross-sections would potentially reveal if this is the case. Under the condition the deviation decreases in a linear relationship with cross-sections spaced in a closer distance e.g. every 1 km along the coastline, according to this the losses during the interpolation procedure are most likely the cause for the offset between 2D and 3D in a homogenous setting. On the other hand, if a deviation of 0.5 % prevails, then it is plausible to account these to the simplification made in terms of dimensionality.

Detailed inspection of the salinization pattern encountered in the homogenous cases indicated an irregular mixing pattern in the saline-fresh mixing zone. As the material is strictly homogenous a clear spatial degraded mixing zone was expected. But this is not the case as certain areas show accumulations of horizontal and vertical variable-density groundwater flow. This phenomenon has been mentioned by previous studies (Goswami et al., 2011; Simmons et al., 2002; Van Damet al., 2009). Irregular vertical and horizontal salinization patterns were encountered in uniform material with identical grain size e.g. in well sorted sand. Most likely spatial variations in solute concentration result in varying buoyancy effects that initiate different flow velocities. Furthermore, the arrangement of grains in different constellations could lead to different pore diameters, thus creating varying pore-scale velocities.

The deviation between 2D and 3D grows considerably larger with inserted geological heterogeneity. The difference in total fresh water volume increases to approximately 2 % and a shift of the salt-fresh interface up to 2.5 km further in the direction of the coastline was observed. Several studies have made similar observations. Kerrou and Renard (2009) found the impact of heterogeneity to vary between 2D and 3D models in magnitude and also general behaviour. Contrary to the results in chapter 4 they found the toe penetration length to reduce in 2D models with increasing random heterogeneity. At the same they conclude variable-density flow can increase but also decrease for 3D models depending on anisotropy and heterogeneity factors. The involvement of the third dimension may influence the effective hydraulic conductivity and effective dispersity. Another factor potentially contribution to the mismatch between 2D and 3D are preferential flow paths on a micro and macro scale which may not be captured by 2D models. The difference in fresh groundwater volumes has been identified to be quite significantly larger between

the homogenous and heterogeneous 3D model scenarios than that of the same configuration of the 2D interpolation. This is coherent with previously mentioned knowledge as the effects of heterogeneity are more likely to cause notable impacts in a 3D setting due to more possibilities for structure related flow paths and spatially varying flow directions based on heterogonous porous material, as well as the like hood to generate instabilities. Influences of connected geomorphology in the dimension neglected in the 2D models may also have an impact in flow characteristics and account to the differences between 2D and 3D models (Abarca, et al., 2007). It should be noted that the layers in the geological model are mostly almost horizontal and don't contain sharp uneven aquifer boundaries with local depressions in the layer bottoms. Therefore, the influence of geomorphology and its variations are limited and could be much higher in specific cases, thus increasing the offset between 2D and 3D model scenarios to a greater degree.

The high impact of local geology on variable-density groundwater flow behaviour highlights the importance a detailed and precise reconstruction of the geological features has on the replicability of real systems through numerical models. Several studies confirm this statement (Ghassemi et al. 2000; Oki et al. 1998; Hodgkinson et al. 2007). The presence of fresh groundwater in the eastern and western flanks of the Bangkok Bay leads to the assumption these areas must have a less permeable top layer creating a greater hydraulic resistance and thus resulting in more freshwater staying present at the top of the system. Though we know this is not the case as Bangkok Clay with an equal total thickness (5 m) was assigned to all areas of the seabed (chapter 3.2.4). Therefore, it has to be attributed to the simplifications made during the conversion from geological to numerical model in which the bulk sediment thickness has a direct influence on the thickness of each individual layer. In these areas the thickness from top to bottom of the system is quite low and ranges between 60 and 90 m. As a result, due to the discretization of 34 layers each layer only has a thickness of approximately 2 to 2.5 m at the mentioned location. For the conversion of geological to numerical model this implies the 2 uppermost layers are assigned with clay of extremely low hydraulic conductivity (4.06 E-05 m/d). Whereas the areas in the central parts of the basin inhibit a total system thickness of up to 500 m, resulting in a layers of 15 m thickness. Considering the thickness of Bangkok Clay it is clear that the hydraulic conductivity was interpolated and averaged out with the underlying sand for these areas as the layer thickness of the geological model is thinner than that of the numerical model. This illustration points out that the hydraulic conductivity values for the eastern part of the bay are as defined in the geological model. Rather than that it hints at too low hydraulic conductivities for the rest of the seabed and indicates the difference between 3D_A and 3D_B would be even greater without simplifications made during transition of geological to numerical model.

Inspection of the upper saline to fresh transition zone has shown fresh groundwater to be present under the seabed far beyond the coastline. A long term simulation has proven it to be prevalent even after 150 kyrs (chapter 4.3.5). The offshore availability of freshwater in direct contact to the systems freshwater recharge indicates submarine ground water discharge (SDG). Groundwater is recharged inland and transported through the connected aquifers onto the continental shelf, where it slowly mixes with seawater and discharges into the sea. In such a case recharge supplies the offshore freshwater and provides an opposing force to intruding variable-density groundwater flow hindering the saline-fresh interface to penetrate towards the coastline.
Recent studies have indicated this phenomenon for multiple global areas. Certain cases have revealed fresh groundwater to be found up to 100 km off the coastline (Post, et al., 2013). As the sea level and with that the coastline is constantly changing in periods of transgression and regression, a

long term simulation with constant boundary conditions as applied in this study does not represent a realistic paleo reconstruction. The salinization process in heterogenous media can take very long time spans depending on the hydraulic resistance. Furthermore, fresh groundwater can be cut off from the groundwater recharge of the system resulitng in a highly complex offshore groundwater distribution with occuring freshwater lenses (Delsman, et al., 2014). The implementation of a detailed paleoreconstruction could provide further insights to the paleohydrological situaiton in the Gulf of Thailand. Apart from that, measurements would have to be conducted to confirm the assumption of SGD being the case for the Gulf of Thailand. Furthermore, it should be noted that the geophysical data used in this study does not provide sufficient coverage of the model area. Therefore the presence of sealing marine clay for the entire seabed of the Gulf of Thailand is highly uncertain. It is likely for the clay layer to have gaps enabling stronger seawater – groundwater interactions, thus resulting in highly different model outcomes.

2. *How noticeable is the influence of rivers in 2D and 3D models; how deep into the aquifer do its influences reach?*

The results indicate 2D and 3D models to deviate in the extent of river-groundwater interactions. For the 3D scenario, the correlation between more freshwater being present with a higher river conductance leads to the assumption that rivers supplying groundwater to the system outweigh those which drain groundwater out of the system. The rivers supply water through infiltration. As a result higher hydraulic heads can be expected in the aquifer, which thereby act as a higher opposing force to intruding variable-density groundwater flow. The 2D models do not follow this trend as there seems to be no linear correlation between river conductance and total fresh groundwater volume. The difference between 2D and 3D in freshwater volume could thereby potentially be attributed to less water being provided by rivers into the system. As river location, river stage and river conductance are identical for both model types, the difference could also be attributed to the distribution of hydraulic heads in the system. Hydraulic heads are calculated by the 2D model itself, therefore a river that provides water in the 3D setting can act draining in the 2D setting due to a higher hydraulic head in the 2D groundwater system.

Another point to consider is the meandering nature of rivers. The orientation of rivers can vary and between orthogonal and parallel to the 2D model. This may result in over- or underestimation of the river influence. It is essentially easier captured through 3D models. In case of a 3D model the depth to which interactions between river and aquifer are noticeable is likely to be much larger as multiple river cells are positioned next to each other initiating accumulative effects on the groundwater aquifer. In case of the 2D model this is not the case. Possibly this contributes to the underestimation of the river influence by 2D models. While a parallel orientation between river and 2D model could potentially result in over estimation, although this could not be observed in the 2D model results. Adaptation of the river conductance for active river cells could assist 2D models to reach a similar river impact as observed in 3D models. This could be implemented by allowing for neighbouring river cells to contribute to the system through an adjusted river conductance depending on their distance to the river cell.

3. *What density of 2D models is necessary to obtain an accurate and plausible overview of the delta comparable to a 3D model?*

The approach in this study utilized a high density of 2D profiles which provided coverage in almost all directions and reduced the typical 2D characteristic for the 2D model interpolation. As a result the area of highest interest for coastal aquifer management, which is immediate to the coastline and

typically ranges several kilometres inland, is covered extremely well by the 2D grids. The analysis of the offset between 2D models showed no improvement or worsening in a direct relationship with the 2D model interval chosen. The fact that the largest offset correlated best in terms of fresh groundwater quantity with the 3D model output seems highly questionable. It appears as most likely that random cross-sections were chosen which happen to represent the model area to a better degree, or in this specific case which underestimate the location of the fresh-saline interface and thus reduce the offset between 2D and 3D modelling scenarios. This analysis could be improved with a greater sample number based on the interpolations with random selection of 2D profiles in defined intervals.

4. *What interpolation method and procedure is reasonable from a statistical, but also computational perspective?*

In consideration of the high computational demand of complex interpolation algorithms (e.g. kriging) the nearest method has proven to provide sufficient results in substantially shorter calculation times. Its success can be attributed to the high density of 2D models in the areas of fresh-saline transitions and their orientation perpendicular to the fresh-saline interface. From a statistical point of view and for cases with less observation points available, a more sophisticated interpolation method which takes multiple observation points into account may be preferable. This is especially relevant for interpolations with greater 2D cross section offsets as the nearest method would result in sharp transitions. A method proven to be suitable for the semi-binary character of saline concentration values in coastal areas is indicator kriging. Indicator kriging could preserve obtained 2D salt concentration values to a higher degree than ordinary kriging and lead way to a better reproduction of the saline-fresh interfaces.

5. *Are 2D models a reasonable approach to access the current situation and capture relevant processes in coastal groundwater systems, more precisely in deltaic areas?*

The previous research questions already addressed the effects of heterogeneity, geomorphology and rivers on both 2D and 3D models and displayed noticeable differences. Wells were not included in this study, but the highly local impact of extractions on the saline-fresh interface is difficult to capture with conventional 2D models. Therefore, it is clear that only one or very few 2D profiles are not feasible to represent present day situations of deltaic areas with an abundance of groundwater extractions and a high influence of river-groundwater interactions. Further deltaic areas often contain complex geological structures with discontinuous clay lenses and spatially varying hydraulic properties due to the depositional environment which often fluctuates between marine and fluviatile/lacustrine conditions.

For this reason we conclude for deltaic areas a 3D approach becomes increasingly necessary. In case of simpler coastal aquifers with less river-groundwater interaction, little influence of extractions and homogenous material covering the large extent of the investigated area a 2D dimensional approach may be feasible. Further the demonstrated approach with multiple 2D models and its consecutive interpolation could be utilized to provide spatial coverage. This technique could be useful to provide an estimate on coastal fresh groundwater quantities and might prove to be suitable for the simulation of very large runtimes. Possibly, paleo-reconstructions for timescales beyond 100 kyrs could be conducted with the simpler and faster 2D approach.

6 Conclusions and outlook

6.1 Conclusion

A three-dimensional variable-density groundwater flow and salt transport model was set up for the Chao Phraya Delta in Thailand using the software iMOD-SEAWAT. Open source data was collected and a 3D geological model was constructed to reproduce the most important geological structures of the sedimentary basin. Additionally to the 3D model, thirty-five 2D models were set up with an offset of 5 km along the coastline using based FloPy-SEAWAT. All 2D models were combined and spatially interpolated using ordinary kriging to cover the 3D model domain. Both 3D and 2D variable-density groundwater flow and salt transport models manage to represent the Chao Phraya River Delta to a similar extent. Variations in total fresh groundwater volume for the entire model domain are measured at below 0.5 % for comparison of a homogenous setting and at less than 2 % for a heterogeneous setting. The great amount and mixed orientation of 2D models in the Gulf of Thailand provides coverage in almost all directions and reduces the typical two dimensional characteristic for the 2D model interpolation. This allows for a good representation of the coastal groundwater system through 2D models which would normally not be the case for 2D studies.

Implementation of the geological model results in significantly different salinization patterns compared to those present in the homogenous model. The scarce geological data required many simplifications to be made. Some of these have major impacts on the outcome of the model. Low saline groundwater resources (<1 TDS g/L) locked beneath low permeable clay layers for the upper layers in the Gulf of Thailand were identified by the 3D model and reproduced, although to a slightly lesser extent, by the 2D models. Simulated offshore freshwater resources have shown to be prevalent even after a time span of 150 thousand years and are directly connected with terrestrial groundwater recharge. The uncertainty of the clay coverage for the seabed of the Gulf of Thailand would require validation measurements to confirm the presence of offshore freshwater.

Salinization patterns in 2D and 3D models show measurable differences. For the two dimensional approach the freshwater-saline interface in the upper layers can be found approximately 2.5 km further in the direction of the coastline. Therefore it seems as though the 2D models slightly overestimate variable-density groundwater flow. This is mainly a consequence of higher dispersion in 3D systems in the direction which is not accounted for in a 2 dimensional approach. On the other hand, the spatial volume of the 3D models gives more space for unstable variable-density processes and therefore can result in the generation of horizontal and vertical salinization patterns with greater spatial extent as seen in the lower parts of the aquifers.

In deltaic areas rivers play a vital role in the systems hydrological cycle and taking in the interactions between groundwater and surface water body can make a massive difference in model outcome. Comparison of river scenarios has shown profound differences between 2D and 3D model implementations. Rivers tend to have higher impacts in the 3D model due to the cumulative effects of neighbouring river cells, which is not the case in 2D models as a result of the restrictions in dimensionality. Therefore, the depth and lateral outreach of rivers is lower in a 2D settings and the generated river influx into the aquifer is underestimated. This results in less freshwater being provided into the groundwater system generating a shift of the saline-fresh interface by pushing more freshwater out of the system.

All in all 2D models have computational advantages over 3D models, but lack the effects of spatial variation in the direction orthogonal to the 2D model. This becomes an increasing factor with the presence of heterogeneity, geomorphology, rivers and local extractions which result in substantially different salinization patterns between 2D and 3D models. Nevertheless, the presented approach utilizing multiple 2D models could be beneficial for the simulation of high runtimes and a swift identification of the fresh-saline interface. But as differences in variable-density groundwater flow behaviour can result in the approximation of the fresh saline interface to vary quite significantly between 2D and 3D it is clear that a 3D approach is preferable. This becomes increasingly relevant for the assessment of scenarios with changes in extraction rates, river influences and land use due to their local impact on the fresh-saline interface.

6.2 Outlook and future work

A) The implementation of a detailed paleoreconstruction could provide insights to the paleohydrological situation. The possibility of fresh water reserves in the offshore area could be investigated.

B) Requesting additional lithological borelog data with the subsequent construction of more detailed geological model could reveal non-continuous layers that enable an enhanced vertical exchange between the aquifers. Previous studies have noted the prevalence of such connections based on contaminates being transported between the aquifers in relevant small times scales, but the local distribution of the gaps remains unknown (Stoecker, et al., 2013).

C) Including wells into the model would provide an interesting perspective on the impact of up-coning and to what degree a 2D model is able to capture such local variations of the saline-fresh interface.

D) Adding anthropogenic induced factors such as land subsidence and hydraulic head drawdown would give way to the simulation of current situation and future scenarios.

E) For regions with climates containing wet and dry season incorporating seasonality into the model could result in significant differences in salt water intrusion.

7 Appendix

7.1 References

Abarca, E., Ramírez, J., Sanchez-Vila, X. & Voss, C., 2007. Quasi-horizontal circulation cells in 3D seawater intrusion. *Journal of Hydrology,* 1 6, Volume 339, pp. 118-129.

Andreadis, K. M., Schumann, G. J.-P. & Pavelsky, T., 2013. A simple global river bankfull width and depth database. *Water Resources Research,* 29 7, 49(10), pp. 7164-7168.

Bakker, M. et al., 2016. Scripting MODFLOW Model Development Using Python and FloPy. *Groundwater.*

Barlow, P. M., 2003. *Ground Water in Freshwater-Saltwater Environments of the Atlantic Coast Circular 1262, USGS*.

Beinhorn, M., Dietrich, P. & Kolditz, O., 2005. 3-D numerical evaluation of density effects on tracer tests. *Journal of Contaminant Hydrology,* 1 12, 81(1-4), pp. 89-105.

C Flowers, T. & R Hunt, J., 2007. Viscous and gravitational contributions to mixing during vertical brine transport in water-saturated porous media. *Water resources research,* 10 1, Volume 43, pp. W01407.1-W01407.18.

Cremer, C. J. M. & Graf, T., 2015. Generation of dense plume fingers in saturated-unsaturated homogeneous porous media. *Journal of Contaminant Hydrology,* Volume 173, pp. 69 - 82.

De Graaf, I. E., Sutanudjaja, E. H., Van Beek, L. P. & Bierkens, M. F., 2015. A high-resolution global-scale groundwater model. *Hydrology and Earth System Sciences,* Volume 19, pp. 823-837.

Delsman, J. R., 2015. *Saline groundwater – Surface water interaction in coastal lowlands.* Amsterdam: IOS Press BV.

Delsman, J. R. et al., 2014. Paleo-modeling of coastal saltwater intrusion during the Holocene: an application to the Netherlands. *Hydrology and Earth System Sciences,* 2 10, 18(10), pp. 3891-3905.

Delsman, J. R. et al., 2016. Global sampling to assess the value of diverse observations in conditioning a real-world groundwater flow and transport model. *Water Resources Research,* Volume 52, pp. 1652 - 1672.

Fick, S. E. & Hijmans, R. J., 2017. WorldClim 2: new 1-km spatial resolution climate surfaces for global land areas. *International Journal of Climatology,* 37(12), pp. 4302-4315.

Flowers, T. C., & Hunt, J. R. (2007). Viscous and gravitational contributions to mixing during vertical brine transport in water-saturated porous media. Water resources research, 43(1), W01407.1-W01407.18.

Frind, E. O., 1982. Seawater intrusion in continuous coastal aquifer-aquitard systems*. *Advances in Water Resources,* Volume 5, pp. 82 - 97.

Ghassemi, F., Alam, K. & Howard, K., 2000. Fresh-water lenses and practical limitations of their three-dimensional simulation. *Hydrogeology Journal,* 8(5), pp. 521-537.

Giao, P., Phien-Wej, N. & Honjo, Y., 1998. FEM quasi-3D modelling of responses to artificial recharge in the Bangkok multiaquifer system. *Environmental Modelling & Software,* 1 12, 14(2-3), pp. 141-151.

Gupta, A. D., 1985. Simulated Salt-Water Movement in the Nakhon Luang Aquifer, Bankgok, Thailand, Groundwater, Volume 23, Issue 4, pp 512-522.

Hartmann, J. & Moosdorf, N., 2012. The new global lithological map database GLiM: A representation of rock properties at the Earth surface. *Geochemistry, Geophysics, Geosystems,* 7 12.13(12).

Hodgkinson, J., Cox, M. E. & McLoughlin, S., 2007. Groundwater mixing in a sand-island freshwater lens: density-dependent flow and stratigraphic controls. *Australian Journal of Earth Sciences,* 1 10, 54(7), pp. 927-946.

Johannsen, K., Oswald, S., Held, R. & Kinzelbach, W., 2006. Numerical simulation of three-dimensional saltwater-freshwater fingering instabilities observed in a porous medium. *Advances in Water Resources,* Volume 81, pp. 89 - 105.

Kerrou, J. & Renard, P., 2010. Analyse numérique des effets dimensionnels et des hétérogénéités sur les intrusions d'eau marine en milieu dispersif. *Hydrogeology Journal,* Issue 18, p. 55– 72.

Knorr, B. et al., 2016. Representativeness of 2D models to simulate 3D unstable variable-density groundwater flow in porous media. *Journal of Hydrology,* 1 11, Volume 542, pp. 541-551.

Kooi, H., Groen, J. & Leijnse, A., 2000. Modes of seawater intrusion during transgressions. *Water Resources Research,* 36(12), pp. 3581-3589.

Langevin, C. D. et al., 2008. *SEAWAT Version 4: A Computer Program for Simulation of Multi-Species Solute and Heat Transport, USGS*.

McDonald, M. G., Harbaugh, A. W., 1988. *A modular three-dimensional finite-difference ground-water flow model, USGS*.

Molle & François, 2005. *The Closure of the Chao Phraya River Basin in Thailand: Its Causes, Consequences, and Policy Implications The Evolution of Supply and Demand Development of Water Resources.*

Mulder, T., 2018. *Constructing 3D variable-density groundwater flow models for six deltas using global data sets,* Department of Physical Geography, Utrecht University.

Nicholls, R. J. et al., 2007. *Coastal systems and low-lying areas: Climate Change 2007: Impacts, Adaptation and Vulnerability. Contribution of Working Group II to the Fourth Assessment Report of the Intergovernmental Panel on Climate Change.* Cambridge, UK, 315-356: Cambridge University Press.

Oki, D. S., Souza, W. R., Bolke, E. L. & Bauer, G. R., 1998. Numerical analysis of the hydrogeologic controls in a layered coastal aquifer system, Oahu, Hawaii, USA. *Hydrogeology Journal,* 6(2), pp. 243-263.

Oki, T. & Kanae, S., 2006. Global Hydrological Cycles and World Water Resources. *Science,* 25 8, 313(5790), pp. 1068-1072.

Oude Essink, G. H., 2001. Improving fresh groundwater supply—problems and solutions. *Ocean & Coastal Management,* 1 1, 44(5-6), pp. 429-449.

Oude Essink, G. H. P., 2001. Salt Water Intrusion in a Three-dimensional Groundwater System in The Netherlands: A Numerical Study. *Transport in Porous Media,* 43(1), pp. 137-158.

Phien-wej, N., Giao, P. & Nutalaya, P., 1998. Field experiment of artificial recharge through a well with reference to land subsidence control. *Engineering Geology,* 1 9, 50(1-2), pp. 187-201.

Phien-wej, N., Giao, P. & Nutalaya, P., 2006. Land subsidence in Bangkok, Thailand. *Engineering Geology,* 2 2, 82(4), pp. 187-201.

Post, V. E. A. et al., 2013. Offshore fresh groundwater reserves as a global phenomenon. *Nature,* 4 12, Volume 504, pp. 71-78.

Post, V. E. et al., 2018. Celebrating 50 years of SWIMs (Salt Water Intrusion Meetings). *Hydrogeology Journal,* 26(6), p. 1767–1770.

Puchała, R. J., Porbski, S. J., Śliwiński, W. R. & August, C. J., 2011. Pleistocene to Holocene transition in the central basin of the Gulf of Thailand, based on geoacoustic survey and radiocarbon ages. *Marine Geology,* Volume 288, Issue 1,pp. 103-111.

Puchała, R. & Porębski, S., 2014. *Morphology and origin of modern seabed features in the central basin of the Gulf of Thailand Morfologia i pochodzenie współczesnych form dna w centralnej części Zatoki Tajlandzkiej*.

Sanford, W. & Buapeng, S., 1996. Assessment Of A Groundwater Flow Model Of The Bangkok Basin, Thailand, Using Carbon-14-Based Ages And Paleohydrology. *Hydrogeology Journal,* 1 4, Volume 4, pp. 26-40.

Sawyer, A. H., David, C. H. & Famiglietti, J. S., 2016. Continental patterns of submarine groundwater discharge reveal coastal vulnerabilities. *American Association for the Advancement of Science,* 353(6300), pp. pp. 705-707.

Shiklomanov, I. (1993) World Water Resources. In: Gleick, P., Ed., Water in Crisis, Oxford, New York.

Simmons, C., R. Fenstemaker, T. & Sharp, J., 2001. *Variable-density groundwater flow and solute transport in heterogeneous porous media: Approaches, resolutions and future challenges, Journal of contaminant hydrology*,Volume 12, pp. 245-275.

Simmons, C. T., 2005. Variable-density groundwater flow: From current challenges to future possibilities. Hydrogeology Journal, Volume 13, pp. 116-119.

Simmons, C. T., Pierini, M. L. & Hutson, J. L., 2002. Laboratory Investigation of Variable-Density Flow and Solute Transport in Unsaturated–Saturated Porous Media. *Transport in Porous Media,* 47(2), pp. 215-244.

Sinsakul, S., 2000. Late Quaternary geology of the Lower Central Plain, Thailand. *Journal of Asian Earth Sciences,* 1 8, 18(4), pp. 415-426.

Stoecker, F. et al., 2013. Hydrogeochemical and isotopic characterization of groundwater salinization in the Bangkok aquifer system, Thailand. *Environmental earth sciences,* 1 2, Volume 68, pp. 749-763.

Thailand WebGIS Geoinformation Sharing System for East and Southeast Asia, url: https://ccop-gsi.org/gsi/thailand/index.php

Van Dam, R. L., Simmons, C. T., Hyndman, D. W. & Wood, W. W., 2009. Natural free convection in porous media: First field documentation in groundwater. *Geophysical Research Letters,* 36(L11403).

Voss, C. I., Simmons, C. T. & Robinson, N. I., 2010. Three-dimensional benchmark for variable-density flow and transport simulation: matching semi-analytic stability modes for steady unstable convection in an inclined porous box. *Hydrogeology Journal, Voume 18, Issue 1, pp. 5-23.*

Weatherall, P. et al., 2015. A new digital bathymetric model of the world's oceans. *Earth and Space Science,* 29 6, 2(8), pp. 331-345.

Werner, A. D. et al., 2013. Seawater intrusion processes, investigation and management: Recent advances and future challenges. *Advances in Water Resources,* Volume 51, pp. 3-26.

Xie, Y., Simmons, C. T., Werner, A. D. & Ward, J. D., 2010. Effect of transient solute loading on free convection in porous media. *Water Resources Research,* 46(W11511).

Zamrsky, D., Oude Essink, G. H. P. & Bierkens, M. F. P., 2018. Estimating the thickness of unconsolidated coastal aquifers along the global coastline. *Earth System Science Data,* 3 9, 10(3), pp. 1591-1603.

7.2 Additional Figures

Model input raster files:

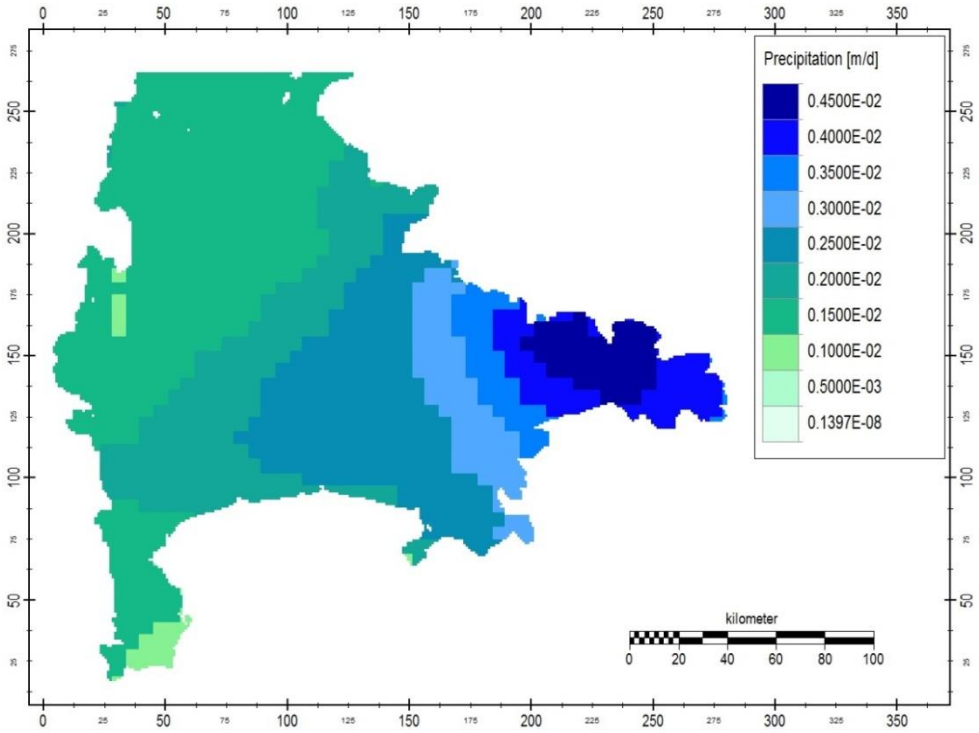

Figure 41: Precipitation based on the WorldClim 2 dataset (Fick & Hijmans, 2017)

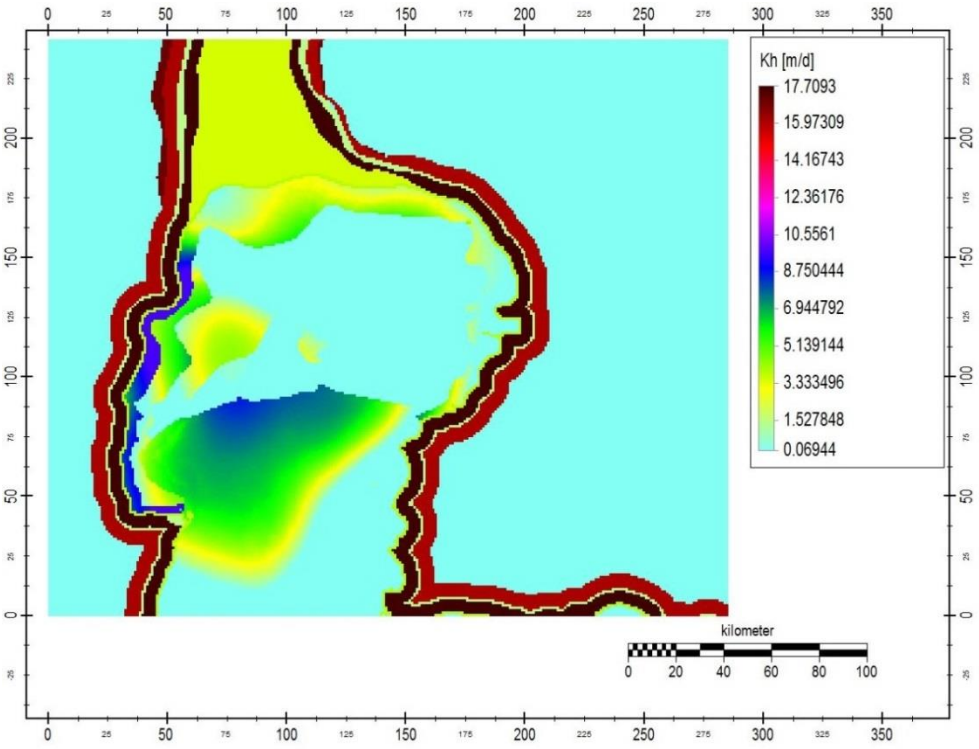

Figure 42: Horizontal hydraulic conductivity values for model layer 1(KH values in m/d)

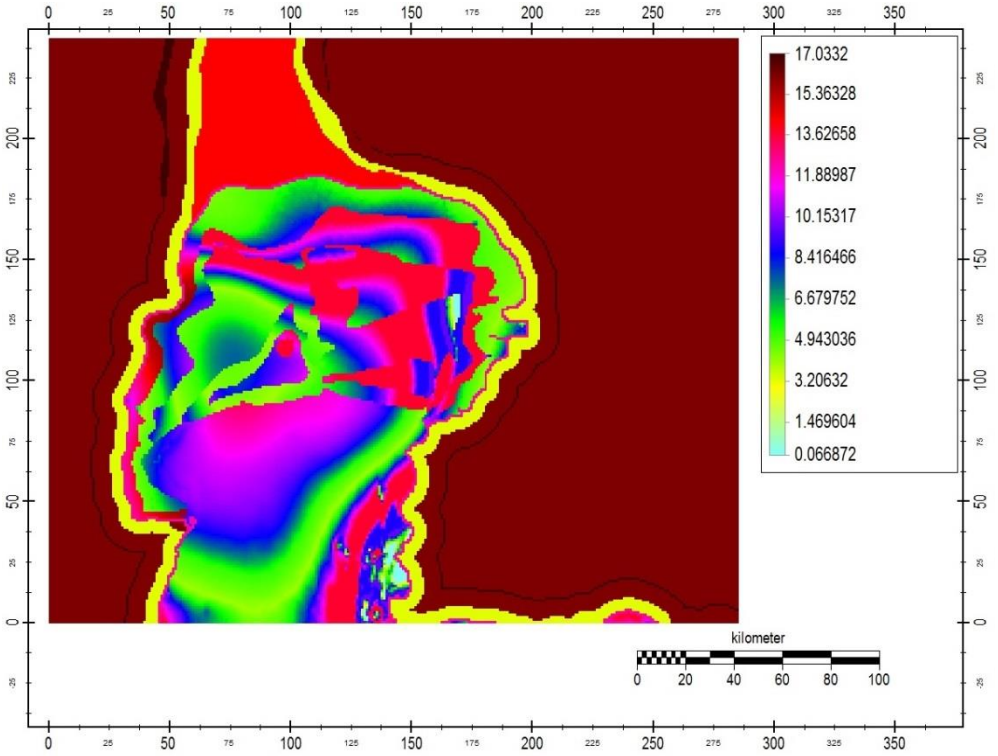

Figure 43: Horizontal hydraulic conductivity values for model layer 5 (KH values in m/d)

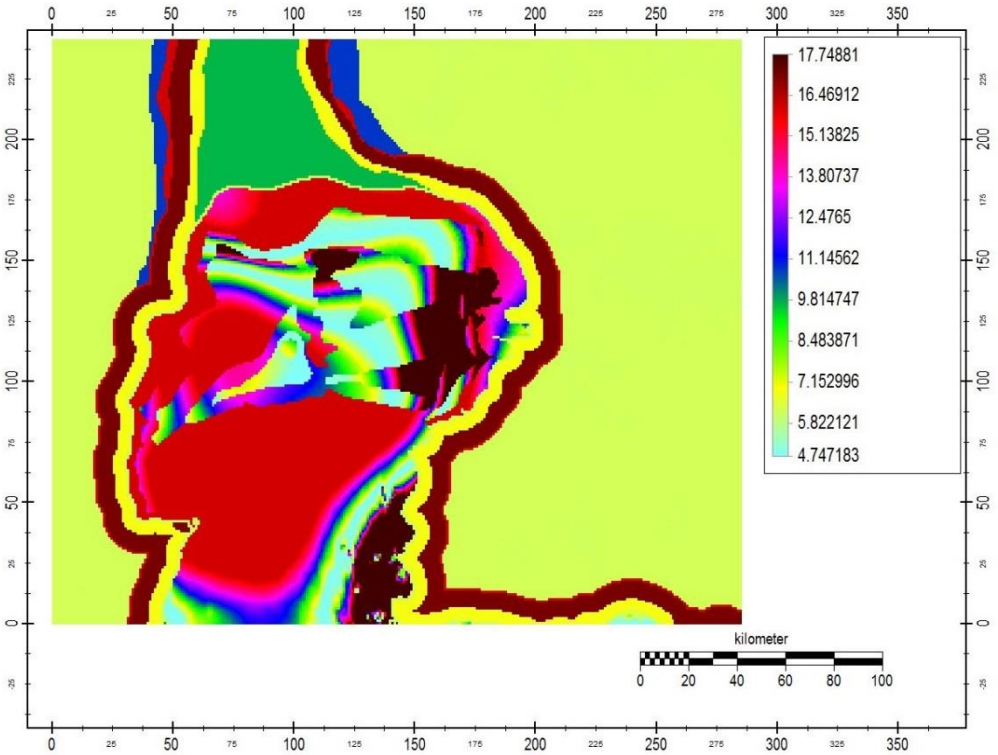

Figure 44: Horizontal hydraulic conductivity values for model layer 10 (KH values in m/d)

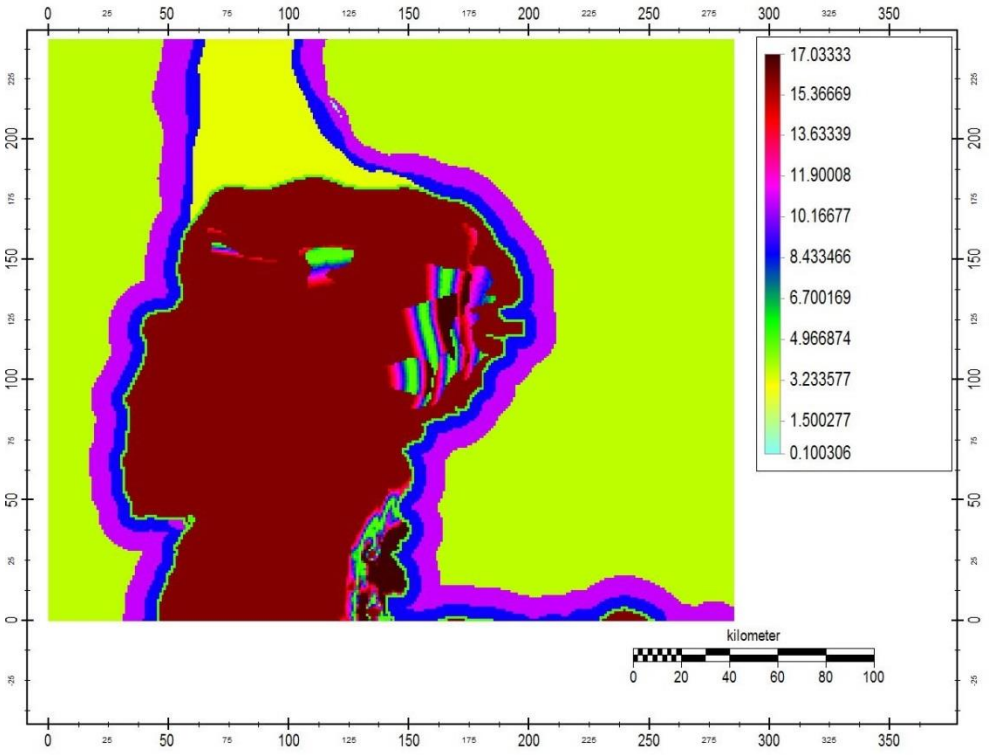

Figure 45: Horizontal hydraulic conductivity values for model layer 20 (KH values in m/d)

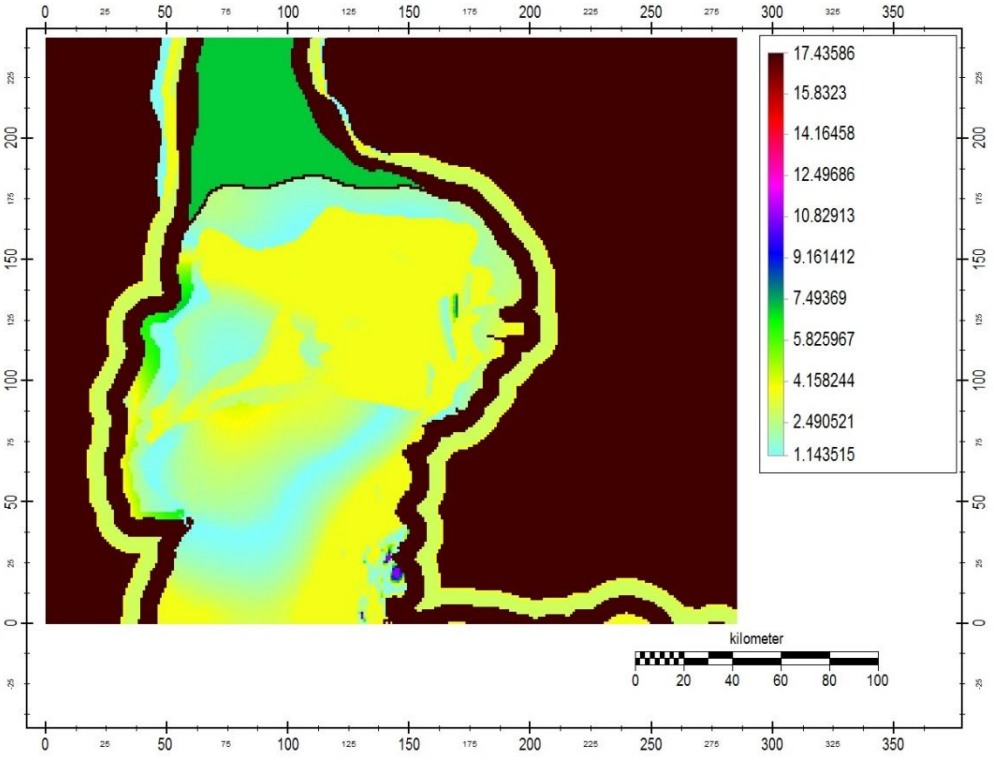

Figure 46: Horizontal hydraulic conductivity values for model layer 30 (KH values in m/d)

Example iMOD-SEAWAT runfile

```
[GEN]                   #General Configuration Package
  MODELNAME = BKK_006_3.2.0_f_2
  WRITEHELP = YES
  RESULT_DIR = .\RESULTS_BKK_001_3.2.0_f_2
  PACKAGES = DIS, BAS6, OC, LPF, GHB, PCG, BTN, ADV, DSP, GCG, SSM, VDF, RCH, RIV, DRN
  COORD_XLL = 0.0                                                    #lower left x-coordinate
  COORD_YLL = 0.0                                                    #lower left y-coordinate
  RUNTYPE = SEAWAT
  START_YEAR = 2000

[DIS]                   #Discretization Package
  NLAY = 34                                                          #amount of layers
  NROW = 266                                                         #amount of rows
  NCOL = 285                                                         #amount of columns
  NPER = 6                                                           #number of stress periods
  DELC_R? = 1000.0                                                   #cell size
  DELR_C? = 1000.0
  TOP = .\IDF_DATABASE\TOP\DEM.IDF                                   #top of the system (raster file: DEM)
  BOTM_L?  = .\IDF_DATABASE\BOT\Layer_?.IDF                          #bottom of each layer
  LAYCBD_L? = 0                                                      #flag for confined aquifer below
  NSTP_P? = 1.
  SSTR_P? = SS                                                       #steady state
  PERLEN_P1 = 0.001                                                  #length of each stress period
  PERLEN_P2 =  365250.0
  PERLEN_P3 =  365250.0
  PERLEN_P4 =  365250.0
  PERLEN_P5 =  365250.0
  PERLEN_P6 =  365250.0
  PERLEN_P7 =  365250.0
  PERLEN_P8 =  365250.0
  PERLEN_P9 =  365249.99

[BAS6]                  Basic Package
  IBOUND_P?_L?=  .\IDF_DATABASE\BND\BND.IDF                          #boundary raster file
  HNOFLO = -9999.                                                    #no data value
  STRT_L?=  .\results_bkk_001_3.2.0_f\head_70000207000000_l?.IDF     #starting heads raster file for each layer


[OC]                    #Output Control Package
  SAVEHEAD_P?_L?  = TRUE                                             #output files
  SAVECONCLAYER_L? = TRUE
  SAVEBUDGET_P?_L? = TRUE
  SAVEHEADTEC_P?_L? = TRUE
  SAVECONCTEC_P?_L? = TRUE
  SAVEVXTEC_P?_L?  = TRUE
  SAVEVYTEC_P?_L?  = TRUE
  SAVEVZTEC_P?_L?  = TRUE
  SAVEHEADVTK_P? = False
  SAVECONCVTK_P? = False
  SAVEVELOVTK_P? = False
  TECFILE = concvelo_2.tec
  PVDFILE = results.pvd

[LPF]                   #Layer Property Package
  HDRY = 1e+30                                                       #head assigned to cells that are converted to dry

  NPLPF = 0
  LAYTYP_L? = 0
  LAYAVG_L? = 0
  CHANI_L? = 1.0
 HK_L? = .\IDF_DATABASE\LPF\mdl_khv_l?.idf                           #horizontal hydraulic conductivity
  VKA_L? * 0.1 = .\IDF_DATABASE\LPF\mdl_khv_l?.idf                   #vertical hydraulic conductivity
  SS_L? = 0.0021                                                     #specific storage coefficient

[GHB]                   #General Head Boundary Package
  MXACTB = 2500000
  IGHBCB = 0
  MGHBSYS = 1
```

```
  BHEAD_P?_S&_L1 = .\IDF_DATABASE\GHB\GHB_NEW\GHB_HEAD_L1.IDF
  BHEAD_P?_S&_L2:34 = .\IDF_DATABASE\GHB\GHB_NEW\GHB_HEAD_L10.IDF
  COND_P?_S&_L1 = .\IDF_DATABASE\GHB\GHB_NEW\GHB_COND_L1_40M_SEA_10M_LAND_0.1.IDF
  COND_P?_S&_L2:34 = .\IDF_DATABASE\GHB\GHB_NEW\GHB_COND_L10_40M_SEA_10M_LAND_0.1.IDF
  GHBSSMDENS_P?_S&_L1 = .\IDF_DATABASE\GHB\GHB_NEW\GHB_DENS_L1.IDF
  GHBSSMDENS_P?_S&_L2:34 = .\IDF_DATABASE\GHB\GHB_NEW\GHB_DENS_L10.IDF

[RCH]                   #Recharge Package
  NRCHOP = 1                                                    #recharge is assigned to the top layer
  IRCHCB = 0
  RCH,INRECH_P?= 1
  RECH_P? *0.03 =  .\IDF_DATABASE\RCH\RCH_0.IDF                 #Recharge idf file

[RIV]                   #River Package
  MXACTR =2500000                                               #max nr. of river reaches
  IRIVCB =0
  MRIVSYS = 1
  STAGE_P?_S&_L1 =  .\IDF_DATABASE\RIV\RIV_STAGE.IDF            #riv stage idf file
  COND_P?_S&_L1 =  .\IDF_DATABASE\RIV\RIV_COND.IDF              #riv conductance idf file
  RBOT_P?_S&_L1 =  .\IDF_DATABASE\RIV\RIV_RBOT.IDF              #riv bot idf file
  RIVSSMDENS_P&_S&_L1 = 1000.

[DRN]                   #Drainage Package
  MXACTD = 2500000
  IDRNCB = 0
  MDRNSYS = 1
  ELEVATION_P?_S?_L1 =  .\IDF_DATABASE\DRN\DRN.IDF              #Drain idf file
  COND_P?_S?_L1  = 1000.0                                       #Drain conductance

[PCG]
  MXITER = 1000                                                 #Maximum number of outer iterations
  ITER1 = 50                                                    #number of inner iterations
  HCLOSE = 0.001                                                #head change criterion for convergence
  RCLOSE = 10000.0                                              #residual criterion for convergence
  RELAX = 0.98                                                  #relaxation parameter
  NBOL = 0
  IPRPCG = 1
  MUTPCG = 1

[BTN]       #Basic Transport Package
  NCOMP = 1
  MCOMP = 1
  DZ_L? =  .\IDF_DATABASE\BOT\THCKNESS_LAYER1.IDF               #discretization (layer thickness)
  ICBUND_L$ =  .\IDF_DATABASE\BND\BND_INACTIVE_ISLANDS.IDF      #Boundary condition idf file
  PRSITY_L$ = 0.3                                               #effective porosity values
  SCONC_T$_L? = .\results_bkk_001_3.2.0_f\conc_70000207000000_l?.IDF  #starting concentration
  CINACT = -9999                                                #no data value
  NPRS = 0
  IFMTCN = 0
  CHKMAS = TRUE
  NPRMAS = 1
  NPROBS = 1
  TSMULT_P? = 1.0
  DT0_P? = 0.0
  MXSTRN_P? = 50000
  TTSMULT_P? = 1.0
  TTSMAX_P? = 0.0

[SSM]                                                           #Sink Source Mixing Package
  MXSS = 25000000                                               # Maximum number of all point sinks and sources
  CRIV_T?_P? = 1e-07                                            #Concentration of rivers
  CRCH_T?_P? = 1e-07                                            #Concentration of recharge
  CGHB_T?_P?_L1 =  .\IDF_DATABASE\GHB\GHB_NEW\GHB_CONC_L1.IDF   #Concentration GHB idf files
  CGHB_T?_P?_L2:34 =  .\IDF_DATABASE\GHB\GHB_NEW\GHB_CONC_L10.IDF

[ADV]                                                           # Advection Package
  MIXELM = 0                                                    # Advection solution option (0=Finite-Difference)
  PERCEL = 1.0

[DSP]                                                           # Dispersion Package
  AL_L? = 5.0                                                   # Longitudinal dispersivity
```

```
   TRPT_L? = 0.1                    # Ratio of horizontal transverse dispersivity to longitudinal dispersivity
   TRPV_L? = 0.1                    # Ratio of vertical transverse dispersivity to longitudinal dispersivity
   DMCOEF_L? = 8.64e-05             # Effective molecular diffusion coefficient

[GCG]                               #Generalized Conjugate Solver Package
   MXITER = 1                       #Maximum outer iterations
   ITER1 = 500                      #Maximum inner iterations
   ISOLVE = 3                       # ,Type of preconditioner used
   CCLOSE = 1e-06                   #Convergence criterion

[VDF]                               #Variable-density groundwater flow Package
  MTDNCONC = 1                      # ,MT3DMS species number that will be used in the equation of state to
                                    compute fluid density
   MFNADVFD = 2
   NSWTCPL = 1
    IWfigure = 0
   DENSEMIN = 1000.0                # Minimum fluid density
   DENSEREF = 1000.0                # Reference fluid density
   DENSEMAX = 1025.                 # Maximum fluid density
   DENSESLP = 0.7143                #The slope d(rho)/d(C) of the linear equation of state that relates solute
                                    concentration for fluid density
```